UNIVERSITAT POLITÈCNICA DE CATALUNYA BARCELONATECH

UPCommons

Portal del coneixement obert de la UPC

http://upcommons.upc.edu/e-prints

Aquesta és una còpia de la versió *author's final draft* d'un article publicat a la revista *Mechanics of materials.*

URL d'aquest document a UPCommons E-prints:

https://upcommons.upc.edu/handle/2117/359063

Article publicat / *Published paper*:

Fontich Julia, E. [et al.]. Critical slowing down close to a global bifurcation of a curve of quasi-neutral equilibria. "Communications in nonlinear science and numerical simulation", 2022, vol. 104, p. 106032:1-106032:21. DOI: 10.1016/j.cnsns.2021.106032

© 2021. Aquesta versió està disponible sota la llicència CC-BY-NC-ND 4.0 https://creativecommons.org/licenses/by-nc-nd/4.0/

Critical slowing down close to a global bifurcation of a curve of quasi-neutral equilibria

Ernest Fontich,[1,*] Antoni Guillamon,[2,3,4] J. Tomás Lázaro,[5,3,4]

Tomás Alarcón,[6,7,4] Blai Vidiella,[8,9,4] and Josep Sardanyés[4,†]

[1]*Departament de Matemàtiques i Informàtica, Universitat de Barcelona (UB), Gran Via de les Corts Catalanes 585, 08007 Barcelona, Spain*

[2]*Departament de Matemàtiques, EPSEB, Universitat Politècnica de Catalunya, Av. Dr. Marañón 44-50, 08028 Barcelona, Spain*

[3]*Institut de Matemàtiques de la UPC-BarcelonaTech (IMTech), Universitat Politècnica de Catalunya, Pau Gargallo 14, 08028 Barcelona, Spain*

[4]*Centre de Recerca Matemàtica. Edifici C. Campus de Bellaterra, 08193 Cerdanyola del Vallès, Barcelona, Spain*

[5]*Departament de Matemàtiques, ETSEIB, Universitat Politècnica de Catalunya, Avda. Diagonal 647, 08028 Barcelona, Spain.*

[6]*ICREA, Pg. Lluís Companys 23, 08010 Barcelona, Spain.*

[7]*Departament de Matemàtiques (Universitat Autonòma de Barcelona). Edifici C. Campus de Bellaterra, 08193 Cerdanyola del Vallès, Barcelona, Spain*

[8]*ICREA-Complex Systems Lab, Universitat Pompeu Fabra, 08003 Barcelona, Spain*

[9]*Institut de Biologia Evolutiva (CSIC-UPF), 08003 Barcelona, Spain*

(Dated: July 3, 2021)

Abstract

Critical slowing down arises close to bifurcations and involves long transients. Despite slowing down phenomena have been widely studied in local bifurcations i.e., bifurcations of equilibrium points, less is known about transients delay phenomena close to global bifurcations. In this paper, we identify a novel mechanism of slowing down arising in the vicinity of a global bifurcation identified in a mathematical model of the dynamics of an autocatalytic replicator with an obligate parasite. Three different dynamical scenarios are first described, depending on the replication rate of cooperators, (L), and of parasites, (K). If $K < L$ the system is bistable and the dynamics can be either the out-competition of the parasite or the two-species extinction. When $K > L$ the system is monostable and both species become extinct. In the case $K = L$ coexistence of both species takes place in a Curve of Quasi-Neutral Equilibria (CQNE) The novel slowing down mechanism identified is due to an underlying *ghost* CQNE for the cases $K \lesssim L$ and $K \gtrsim L$. We show, both analytically and numerically, that the delays caused by the ghost CQNE follow scaling laws of the form $\tau \sim |K-L|^{-1}$ for both $K \lesssim L$ and $K \gtrsim L$. We propose the ghost CQNE as a novel transient-generator mechanism in ecological systems.

*Corresponding author: E. Fontich (fontich@ub.es).

†Corresponding author: J. Sardanyés (jsardanyes@crm.cat).

Keywords: *Bifurcations; Critical slowing down; Ghosts; Normally Hyperbolic Invariant Manifolds; Parasites; Quasi-neutral equilibria; Scaling laws*

I. INTRODUCTION

Bifurcations are responsible for qualitative changes in dynamical systems due to parameter changes [1, 2]. Generically, bifurcations can be classified as local or global. Local bifurcations involve fixed points, which can suffer changes of stability or collisions between them. Classical examples of local bifurcations are transcritical, saddle-node, pitchfork, or Hopf-Andronov bifurcations [1]. Bifurcations play a key role in population dynamics models [3–11] since they often involve species' extinctions. Further theoretical research in biological and socioecological systems has revealed bifurcation phenomena [12–17]. Bifurcations have also been found in a wide variety of models of physical systems, including elastic-plastic materials [18], electronic circuits [19], or open quantum systems [20]. More importantly, bifurcations have been experimentally shown in physical [21–24], chemical [25, 26], and biological systems [27, 28].

One of the most remarkable properties of systems approaching a local bifurcation is that transient relaxations suffer a slow down. The duration of these transients typically scales with the distance to the bifurcation value [2, 29]. Such scaling behavior is found in continuous-time (flows) and discrete-time (maps) dynamical systems alike. For instance, the duration of transients, τ, in transcritical bifurcations diverges as a power law $\tau \sim |\mu - \mu_c|^{-1}$, $\mu > \mu_c$ [29, 30], with μ and μ_c being, respectively, the bifurcation parameter and the bifurcation value. The same scaling exponent is found in the supercritical Pitchfork bifurcation in flows [29], and in the Pitchfork and period-doubling bifurcation in maps [30]. For the saddle-node bifurcation the delay scales as $\tau \sim |\mu - \mu_c|^{-1/2}$ for flows and maps [2, 31, 32] (see also [22] for experimental evidence of this power law in an electronic circuit). The same scaling exponent has been recently found in a delayed differential equation undergoing a saddle-node bifurcation [33].

Global bifurcations involve objects with dimension greater than 0 in the phase space, such as invariant curves, periodic orbits, tori, or strange attractors. Well-known global bifurcations are the saddle-node bifurcation of periodic orbits, both the homoclinic and heteroclinic bifurcations [1], or the so-called chaotic crisis (originally labeled as fusion of strange attractors [34]), where a strange chaotic attractor collides with another object such as an unstable periodic orbit [35] or a chaotic saddle [36]. Chaotic crises are responsible for transient chaos, given by a chaotic orbit that asymptotically achieves another type of attractor. The average lifetime of transient chaos, τ, also follows an algebraic scaling law of the form $\tau \sim (\mu - \mu_c)^{-h}$, with $h > 0$ [35, 37]. The so-called superpersistent chaotic transients also display scaling behaviour, now being of the form $\tau \sim \exp(C\,(p - p_c)^{-\nu})$, with $C > 0$ and $\nu > 0$. This latter type of transient chaos is known to occur

through an unstable-unstable pair bifurcation, in which an unstable periodic orbit inside a chaotic attractor collides with another unstable periodic orbit on the basin boundary [37, 38]. Global bifurcations have been also reported experimentally. For instance, homoclinic bifurcations have been identified in semiconductor lasers [39]. Evidences of transient chaos have been found in radio wave amplification by stimulated emission of radiation (NMR laser) [40] and in spin-wave experiments [41].

Recent research on population dynamics has focused on the so-called quasi-neutral curves, which are one-dimensional invariant objects with attracting and neutral directions. In some cases, these manifolds fall into the class of Normally Hyperbolic Invariant Manifolds (NHIM) [42–44]. Quasi-neutral manifolds have been investigated in the dynamics of allele fixation [45, 46], in two-species Lotka-Volterra models [47] and in models of sexual in diploid populations [48, 49]. These manifolds have been also studied analytically and computationally in epidemiology [50] and in RNA viruses with different replication modes ranging between geometric and stamping machine modes [51]. Quasi-neutral curves imply coexistence within the phase space with different equilibrium states for different initial conditions. CQNE are formed by a continuum of equilibrium values: once an orbit reaches the CQNE, the dynamics stops. This dynamics is fundamentally altered in the presence of noise, which have been also been an important subject of recent research in the context of noise-induced bistability [47, 50, 51].

In this article we focus on the deterministic dynamics close to a global bifurcation involving a CQNE. In this case, if we take away an arbitrarily small neighbourhood of a degenerate point, the CQNE is the union of two different NHIMs. Despite the dynamics on this quasi-neutral manifold is trivial, interesting transient phenomena arise close to the bifurcation. We explore this subject in a system describing the dynamics of two competing replicators including cooperation (autocatalysis) and obligate parasitism. Three dynamical regimes are observed depending on the fitness (replication rates) of the autocatalytic replicator, L, and the parasite, K: (i) when $K > L$ the autocatalytic species is able to out-compete the parasite in a bistable regime including co-extinction; (ii) in the borderline case, $K = L$, the system has a continuum of stable equilibrium points with one stable and one neutral directions, which involves the survival of both species in an structurally unstable scenario; and, last, (iii) when $K > L$, both species become co-extinct in a monostable regime. The shift from scenario (i) to (iii) and vice versa is governed by a global bifurcation, which is degenerate, and involves a remnant CQNE. That is, for values of fitness extremely close to the bifurcation value, the species experience extremely long transients as they are captured by a ghost CQNE. The internal nullclines of the system become very close and glued to the CQNE. The flow passes throughout a bottleneck region in the phase plane causing such delays. We identify and analytically prove scaling laws of the form $\tau \sim |\mu|^{-1}$ (with $\mu := K - L$), close to the bifurcation and for some initial conditions. The detailed results are contained in Theorems 1 and 2.

II. MATHEMATICAL MODEL AND RESULTS

We start by defining a dynamical system describing the population dynamics of two competing species including cooperation and parasitism. The specific system considers an autocatalytic replicator, x, and an obligate parasite y of the autocatalytic replicator. That is, species y receives catalysis from x but does not reciprocate such catalysis, while species x enhances its own replication. The system, only considering replication and decay processes, follows the next reactions:

$$x + x \xrightarrow{L} 3x, \tag{1}$$

$$x + y \xrightarrow{K} x + 2y, \tag{2}$$

$$x \xrightarrow{\gamma} \phi, \tag{3}$$

$$y \xrightarrow{\gamma} \phi. \tag{4}$$

Reaction (1) corresponds to the non-linear (density-dependent) reproduction of the autocatalytic replicator x, which is proportional to a constant $L > 0$. Reaction (2) denotes the catalytic aid that species x provides for the growth of species y, which is proportional to a constant $K > 0$. Finally, reactions (3)-(4) are the density-independent decay of species x and y, respectively, which occur at rate $\gamma > 0$.

The reactions above, involving processes of competition between species (see below), can be modelled by:

$$\frac{dx}{dt} = L x^2 \left(1 - \frac{x+y}{C}\right) - \gamma x, \tag{5}$$

$$\frac{dy}{dt} = K x y \left(1 - \frac{x+y}{C}\right) - \gamma y. \tag{6}$$

Here the growth of the population is constrained by the logistic term $1-(x+y)/C$, which introduces intra-specific competition ($C > 0$ being the carrying capacity) and bounds the growth of the system.

We will call F the vector field that defines system (5)–(6). The state variables x, y span the phase space

$$\Sigma^0 := \{(x,y) \in \mathbb{R}^2 \,|\, x \geq 0, y \geq 0\}.$$

Since $\dot{x} + \dot{y} = (Lx + Ky)x\left(1 - \frac{x+y}{C}\right) - \gamma(x+y) < 0$ if $x + y \geq C$, we have that the orbits with initial conditions $(x_0, y_0) \in \Sigma^0$ arrive at $x + y < C$ after some time. For this reason we restrict the system to the domain

$$\Sigma := \{(x,y) \in \Sigma^0 | \, x + y \leq C\}.$$

Moreover, notice that the axes $\{x = 0\}$, $\{y = 0\}$ are invariant and therefore Σ is positively invariant. It is noteworthy that the sign of the parameter $\mu := K - L$ determines different scenarios that reflect the

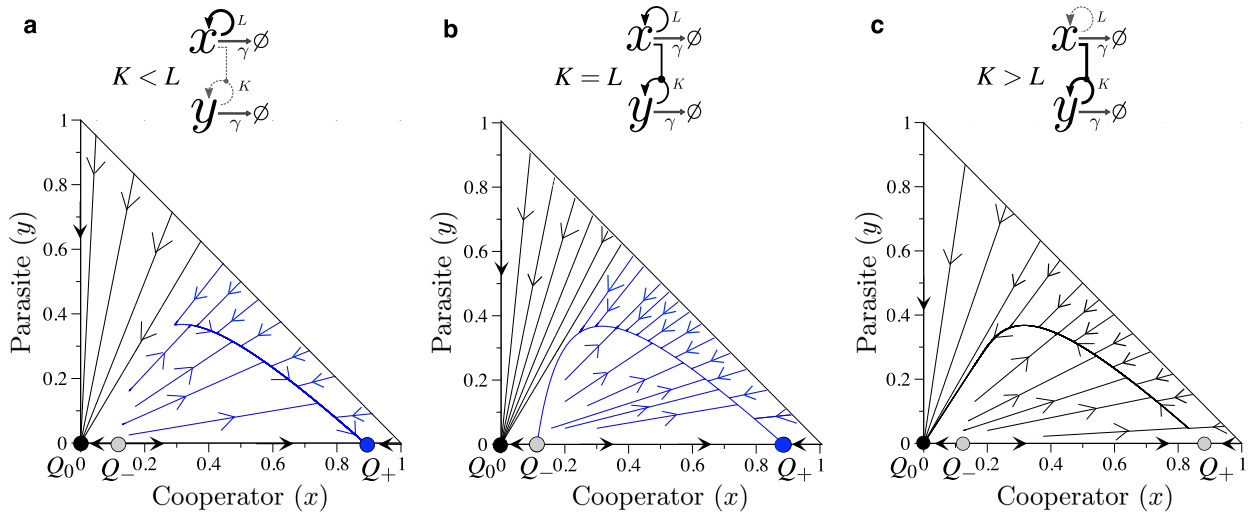

FIG. 1: Different dynamical regimes obtained from Eqs. (5)-(6) with $\gamma = 0.1$. (a) When cooperators replicate faster than parasites (here with $K = 0.995$ and $L = 1$) two possible scenarios are found. Co-extinction (given by equilibrium Q_0) or only survival of the cooperator and extinction of the parasite (equilibrium Q_+) depending on the initial conditions. Notice that a saddle point Q_- is inbetween both equilibria. (b) When both species replicate at the same rates (here with $K = L = 1$), bistability is also found, now with co-extinction or coexistence along the quasi-neutral curve $\mathscr{Q}$, i.e., different initial conditions within the coexistence basis give place to different coexistence equilibria. (c) When parasites replicate faster than the autocatalytic species (here with $K = 1.0005$ and $L = 1$), both species become asymptotically extinct. Unstable equilibria are represented by gray circles, attractors in black (Q_0) and blue (Q_+) circles.

predominance of the catalytic aid from x to y over the autocatalytic replication of x or vice versa. We refeer to Figure 1, upper row, for a schematic representation of these scenarios. A detailed look to the phase portraits shown in Figure 1, from left to right, reveals a change of direction of the flow on an apparently invariant parabola-like curve. This fact suggests a slowing down of the flow for small values of $|\mu|$. In this section, we describe how the passage times close to this distinguished curve scale with parameter μ and we provide analytical proofs of this phenomenon. In Section II A, we give the basic notation and study the equilibrium points of the system and their stability. In Section II B, we underline general dynamical features and study the invariant manifolds of the saddle points. Finally, Section II C contains the main results about the critical slowing down observed in the system close to bifurcation thresholds.

A. Nullclines, equilibrium points and stability

In order to define the nullclines and equilibria (see Figure 2 for a comprehensive plot), we rewrite system (5)–(6) as

$$\dot{x} = Lx^2\,(g_v(x)-y)\,/C, \tag{7}$$

$$\dot{y} = Kxy\,(g_h(x)-y)\,/C, \tag{8}$$

where

$$g_v(x) = C - x - \frac{\gamma C}{L}\frac{1}{x} \qquad \text{and} \qquad g_h(x) = C - x - \frac{\gamma C}{K}\frac{1}{x}. \tag{9}$$

Functions g_v and g_h vanish at the points $\delta_\pm$ and $\xi_\pm$, respectively, with

$$\delta_\pm = \frac{C \pm \sqrt{C^2 - 4\gamma C/L}}{2} \qquad \text{and} \qquad \xi_\pm = \frac{C \pm \sqrt{C^2 - 4\gamma C/K}}{2}. \tag{10}$$

Therefore, we can write

$$g_v(x) = C - x - \frac{\gamma C}{L}\frac{1}{x} = \frac{-1}{x}(x-\delta_+)(x-\delta_-), \tag{11}$$

$$g_h(x) = C - x - \frac{\gamma C}{K}\frac{1}{x} = \frac{-1}{x}(x-\xi_+)(x-\xi_-). \tag{12}$$

Moreover, both functions have a unique maximum at

$$x_v = \sqrt{\frac{\gamma C}{L}} \qquad \text{and} \qquad x_h = \sqrt{\frac{\gamma C}{K}}, \tag{13}$$

respectively, which satisfy

$$g_v(x_v) = C - 2\sqrt{\frac{\gamma C}{L}} \qquad \text{and} \qquad g_h(x_h) = C - 2\sqrt{\frac{\gamma C}{K}}.$$

The vertical nullcline is $\mathcal{N}_v = \{(x,y) \in \Sigma \,|\, \dot{x} = 0\}$ and can be decomposed as $\mathcal{N}_v = \mathcal{N}_v^1 \cup \mathcal{N}_v^2$ with

$$\mathcal{N}_v^1 = \{(x,y) \in \Sigma \,|\, x = 0\}$$

and

$$\mathcal{N}_v^2 = \Big\{(x,y) \in \Sigma \,|\, y = g_v(x)\Big\}.$$

Note that $\mathcal{N}_v^2 \cap \Sigma \neq \emptyset$ if and only if $\gamma \leq CL/4$. Moreover, $\mathcal{N}_v^2$ is below the line $x+y=C$.

Analogously, the horizontal nullcline is $\mathcal{N}_h = \{(x,y) \in \Sigma \,|\, \dot{y} = 0\} = \mathcal{N}_h^1 \cup \mathcal{N}_h^2$ with

$$\mathcal{N}_h^1 = \{(x,y) \in \Sigma \,|\, y = 0\}$$

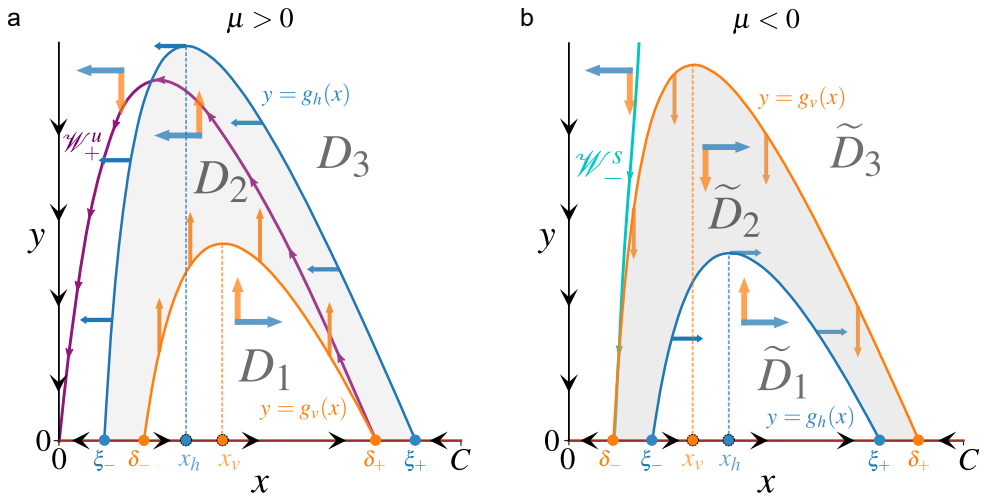

FIG. 2: Nullclines, equilibrium points and relevant regions for $\mu > 0$ (left) and $\mu < 0$ (right). Both axes are invariant and part of the nullclines, which are completed with the curves $\mathscr{N}_h^2$ and $\mathscr{N}_v^2$, defined respectively by $y = g_h(x)$ and $y = g_v(x)$. The maxima of these graphs are attained at $x = x_h$ and $x = x_v$, respectively. Equilibrium points are located at the origin and at the points $Q_\pm = (\delta_\pm, 0)$. In magenta, we show the unstable manifold of Q_+, $\mathscr{W}^u_+$ (panel a, case $\mu > 0$), and the stable manifold of Q_-, $\mathscr{W}^s_-$ (panel b, case $\mu < 0$).

and

$$\mathscr{N}_h^2 = \Big\{(x,y) \in \Sigma \,|\, y = g_h(x)\Big\}.$$

Similarly, $\mathscr{N}_h^2 \cap \Sigma \neq \emptyset$ if and only if $\gamma \leq CK/4$, and it lies below the line $x + y = C$.

The equilibrium points are located at the intersection of the nullclines. We have $\mathscr{N}_v^1 \cap \mathscr{N}_h^1 = \{Q_0\}$, with $Q_0 = (0,0)$. If $\gamma \leq CL/4$, we have that

$$\mathscr{N}_v^2 \cap \mathscr{N}_h^1 = \{Q_-, Q_+\},$$

with $Q_\pm = (\delta_\pm, 0)$, see again Figure 2.

If $\gamma > CL/4$, $\mathscr{N}_v^2 = \emptyset$. The intersection $\mathscr{N}_v^1 \cap \mathscr{N}_h^2$ is always void; moreover, $\mathscr{N}_v^2$ and $\mathscr{N}_h^2$ (when they are not void) coincide for $K = L$ and are disjoint otherwise. Thus, when $K = L$ and $\gamma < CL/4$ we have a curve $\mathscr{Q}$ of equilibrium points $Q_c = (x_c, y_c)$, with $\delta_- \leq x_c \leq \delta_+$, that contains $Q_\pm$ at its endpoints. Moreover, in this case, $\xi_- = \delta_-$ and $\xi_+ = \delta_+$.

The stability analysis of the equilibria will be carried out using the derivative of the vector field. For our system,

$$DF(x,y) = \begin{pmatrix} 2Lx\left(1 - \frac{x+y}{C}\right) - \frac{L}{C}x^2 - \gamma & -\frac{L}{C}x^2 \\ \\ Ky\left(1 - \frac{x+y}{C}\right) - \frac{K}{C}xy & Kx\left(1 - \frac{x+y}{C}\right) - \frac{K}{C}xy - \gamma \end{pmatrix}.$$

Let $\lambda_0^{(1)}$ and $\lambda_0^{(2)}$ be the eigenvalues of $DF(Q_0)$, $\lambda_\pm^{(1)}$ and $\lambda_\pm^{(2)}$, the eigenvalues of $DF(Q_\pm)$, and $\lambda_c^{(1)}$ and $\lambda_c^{(2)}$, those corresponding to $DF(Q_c)$.

It is clear that $\lambda_0^{(1)} = \lambda_0^{(2)} = -\gamma$, and therefore Q_0 is an attractor. Concerning $Q_\pm = (\delta_\pm, 0)$, we notice that $L\delta_\pm(1-\delta_\pm/C) = \gamma$. We have

$$DF(Q_\pm) = \begin{pmatrix} \gamma - \frac{L}{C}\delta_\pm^2 & -\frac{L}{C}\delta_\pm^2 \\ \\ 0 & \left(\frac{K}{L}-1\right)\gamma \end{pmatrix}. \tag{14}$$

Note that

$$\lambda_\pm^{(1)} = \gamma - \frac{L}{C}\delta_\pm^2 = 2\gamma - L\delta_\pm,$$

and it can be shown (when $\gamma < CL/4$) that $\lambda_-^{(1)} > 0$ and $\lambda_+^{(1)} < 0$ (see Lemma 3). Moreover, $\langle (1,0) \rangle$ is always the eigenspace associated to the eigenvalues $\lambda_\pm^{(1)}$. On the other hand,

$$\lambda_\pm^{(2)} = \left(\frac{K}{L} - 1\right)\gamma.$$

The corresponding eigenspace is $\langle (1, m_\pm) \rangle$, where

$$m_\pm := -1 + \frac{\gamma C}{L\delta_\pm^2}\left(2 - \frac{K}{L}\right).$$

Consider now the points Q_c, which are equilibrium points only when $K = L$. We can write

$$Q_c = (x_c, y_c) = \left(x_c\,, C - x_c - \frac{\gamma C}{L}\frac{1}{x_c}\right), \qquad \delta_- \le x_c \le \delta_+,$$

where (x_c, y_c) satisfies

$$L x_c \left(1 - \frac{x_c + y_c}{C}\right) = \gamma.$$

Then

$$DF(Q_c) = \begin{pmatrix} \gamma - \frac{L}{C}x_c^2 & -\frac{L}{C}x_c^2 \\ \\ \gamma\frac{y_c}{x_c} - \frac{L}{C}x_c y_c & -\frac{L}{C}x_c y_c \end{pmatrix}. \tag{15}$$

It is not difficult to check that $\det DF(Q_c) = 0$. This means that an eigenvalue $\lambda_c^{(1)} = 0$. The other one, $\lambda_c^{(2)}$, can be obtained from the trace of $DF(Q_c)$:

$$\lambda_c^{(2)} = \gamma - \frac{L}{C}x_c(x_c + y_c) = 2\gamma - L x_c.$$

To summarize, Q_0 is always an attractor and, whenever it exists, Q_- is a repeller if $K > L$ and a saddle point if $K < L$. The equilibrium Q_+ is a saddle point if $K > L$ and an attractor if $K < L$, whereas Q_c always has a neutral direction plus one unstable direction if $\delta_- \leq x_c < 2\gamma/L$ or one stable direction if $\delta_+ \geq 2\gamma/L < x_c$. Finally, when $x_c = 2\gamma/L$, Q_c is neutral and $DF(Q_c)$ is conjugated to

$$\begin{pmatrix} 0 & 1 \\ 0 & 0 \end{pmatrix}. \tag{16}$$

B. On the dynamics and the invariant manifolds of the saddle points

It is noteworthy that, since the equilibrium points lay on an invariant line, by the Poincaré-Bendixson theorem the vector field cannot have limit cycles. We consider three cases.

1. Case $K > L$ (left panel, Figure 2). When $\gamma < \frac{CL}{4}$, $Q_+ = (\delta_+, 0)$ exists and is a saddle point. It has a one-dimensional unstable manifold $\mathscr{W}_+^u$ tangent to the eigenvector $(1, m_+)$ of eigenvalue $\lambda_+^{(2)} > 0$. To locate $\mathscr{W}_+^u$ we determine a subdomain in wich it is contained. Note first that on $\mathscr{N}_v^2$, $\dot{x} = 0$ and $\dot{y} = \gamma y\left(\frac{K}{L} - 1\right) > 0$, and on $\mathscr{N}_h^2$, $\dot{x} = \gamma x\left(\frac{L}{K} - 1\right) < 0$, and $\dot{y} = 0$. Also $\mathscr{N}_h^2$ is above $\mathscr{N}_v^2$. We introduce

$$\begin{aligned} D_1 &= \{(x,y) \in \Sigma \mid 0 < y < g_v(x)\}, \\ D_2 &= \{(x,y) \in \Sigma \mid g_v(x) < y < g_h(x)\}, \\ D_3 &= \{(x,y) \in \Sigma \mid y > g_h(x)\}. \end{aligned}$$

   From system (7)-(8) we have that, on D_1, $\dot{x} > 0$ and $\dot{y} > 0$; on D_2, $\dot{x} < 0$ and $\dot{y} > 0$; and, on D_3, $\dot{x} < 0$ and $\dot{y} < 0$.

   We now compute

$$g_v'(\delta_+) = -1 + \frac{\gamma C}{L}\frac{1}{\delta_+^2} = -2 + \frac{C}{\delta_+}$$

   and compare it with the slope of the eigenvector at Q_+: $m_+ < g_v'(\delta_+) < 0$. Then, close enough to Q_+, $\mathscr{W}_+^u$ has to stay in D_2. In D_2, the y-component of $\mathscr{W}_+^u$ increases as x decreases until it meets ∂D_3 and enters into D_3 when its tangent vector is horizontal; at this point, the invariant manifold reaches a maximum since in D_3 one has $\dot{y} < 0$. In D_3, $\mathscr{W}_+^u$ decreases monotonically towards the origin, the only possible ω-limit (see then magenta curve in Figure 2 and the red curve in Figure 4(a,c)).

2. Case $K = L$. In this case all straight lines through the origin are invariant. Indeed, the vector field

evaluated on $(x,\alpha x)$ is

$$F(x,\alpha x)=\begin{pmatrix} Lx^2\left(1-\frac{x+\alpha x}{C}\right)-\gamma x \\ \\ L\alpha x^2\left(1-\frac{x+\alpha x}{C}\right)-\gamma\alpha x \end{pmatrix} =: \begin{pmatrix} \tilde{x} \\ \\ \alpha\tilde{x} \end{pmatrix},$$

from some $\tilde{x}$.

If we restrict the vector field to any of such lines we see that, apart from the origin, and provided that

$$0\leq\alpha<\frac{CL}{4\gamma}-1,$$

the restriction has two equilibrium points; if $\alpha=\frac{CL}{4\gamma}-1$, only one equilibrium point exists; and, if $\alpha>\frac{CL}{4\gamma}-1$, it has no equilibrium points.

3. Case $K<L$, see right panel of Figure 2. Now $\mathscr{N}_v^2$ is above $\mathscr{N}_h^2$. We introduce

$$\begin{aligned}\widetilde{D}_1 &= \{(x,y)\in\Sigma \mid 0<y<g_h(x)\},\\ \widetilde{D}_2 &= \{(x,y)\in\Sigma \mid g_h(x)<y<g_v(x)\},\\ \widetilde{D}_3 &= \{(x,y)\in\Sigma \mid y>g_v(x)\}.\end{aligned}$$

On $\widetilde{D}_1$ we have $\dot{x}>0,\dot{y}>0$; on $\widetilde{D}_2$ we have $\dot{x}>0,\dot{y}<0$; and on $\widetilde{D}_3$ we have $\dot{x}<0,\dot{y}<0$. The equilibrium point Q_- becomes a saddle point whose one-dimensional stable invariant manifold $\mathscr{W}_-^s$ is tangent at Q_- to $(1,m_-)$. Comparing this vector with the derivative

$$g_v'(\delta_-)=-1+\frac{\gamma C}{L}\frac{1}{\delta_-^2}=-2+\frac{C}{\delta_-}>0,$$

we see that

$$m_->g_v'(\delta_-)>0. \tag{17}$$

Therefore, close enough to Q_-, the manifold $\mathscr{W}_-^s$ stays in $\widetilde{D}_3$. It cannot enter into $\widetilde{D}_2$ and remains in $\widetilde{D}_3$ until it meets $\{x+y=C\}$ (see right panel of Figure 2).

The results described above are illustrated in Figure 1 by means of phase portraits numerically built using a fourth-order Runge-Kutta method with a constant time step-size $\Delta t=0.01$. Panel (a) shows several orbits for the case $K<L$. Here, the orbits can reach two different attractors depending on the initial conditions. For low population values of cooperators and large numbers of parasites, the full system becomes extinct reaching equilibrium point Q_0, which is locally asymptotically stable. The case in which the parasite replicates faster than the autocatalytic species $(K>L)$ involves the full extinction for $y(0)>0$, since Q_+

is a saddle point whose upper branch of the unstable manifold enters into D_2. Finally, as mentioned, when both species replicate at the same rates, a quasi-neutral curve $\mathscr{Q}$ appears, involving different equilibrium values for species' coexistence depending on the initial conditions within the basin of attraction of the curve. Notice that here the equilibrium Q_0 maintains a basin of attraction.

C. Dynamics close to bifurcation thresholds

In this section we will focus on the dynamics arising close to the global bifurcation occurring at $K = L$, which corresponds to the bifurcation value $\mu = 0$. We will investigate the case $\mu \gtrsim 0$, which involves a single asymptotic dynamics i.e., co-extinction. The slowing down for this case depends on the initial conditions. Then, we will focus on the dynamics for $\mu \lesssim 0$, which results in either survival of the autocatalytic replicator and extinction of the parasite, or co-extinction, depending on the initial conditions. We note here that the slowing down will occur for those initial conditions approaching the ghost CQNE, thus involving the survival of the autocatalytic species alone. We first provide numerical results to illustrate the dynamics as the bifurcation is approached. Then, we derive analytically the scaling laws relating the passage times with the parametric distance to the bifurcation value.

1. Numerical results

We first provide a numerical study of the dynamics for $\mu \gtrsim 0$. Figure 3(a) displays the times that the system spends to reach Q_0 for different initial conditions. For $\mu = 0.5$ the dynamics is fast because the nullclines $\mathscr{N}_h^2$ (black) and $\mathscr{N}_v^2$ (gray) are separated. As $\mu \to 0$, both nullclines get close, almost coinciding with the manifold $\mathscr{W}_+^u$, causing an extremely long passage of the orbits. Note that for $\mu = 5 \times 10^{-4}$, initial conditions involving low (large) population of parasites (autocatalytic species) cause the orbits to approach this unstable manifold, which is weakly hyperbolic. This makes transients to become extremely slow. This is illustrated in Figure 4 for the cases $\mu = 0.5$ (panel (a)) and $\mu = 5 \times 10^{-4}$ (panel (b)) by means of phase portraits and time series. The case $\mu = 0.5$ implies a fast dynamics in which the orbits approach $\mathscr{W}_+^u$ and flow towards extinction. Five time series are displayed in panel (b) and (d). The chosen initial conditions are indicated with coloured circles. Notice that extinction times are short. For $\mu = 5 \times 10^{-4}$, the dynamics experience extremely long delays, especially at low initial populations of parasites and increasing initial populations of the autocatalytic species. That is, for those initial conditions within the basin of attraction of the $\mathscr{Q}$ curve for $\mu = 0$, the time series experiences a very long delay (ghost transient) before extinction. As it occurs with local bifurcations, we have identified a power-law scaling relation between the length of the

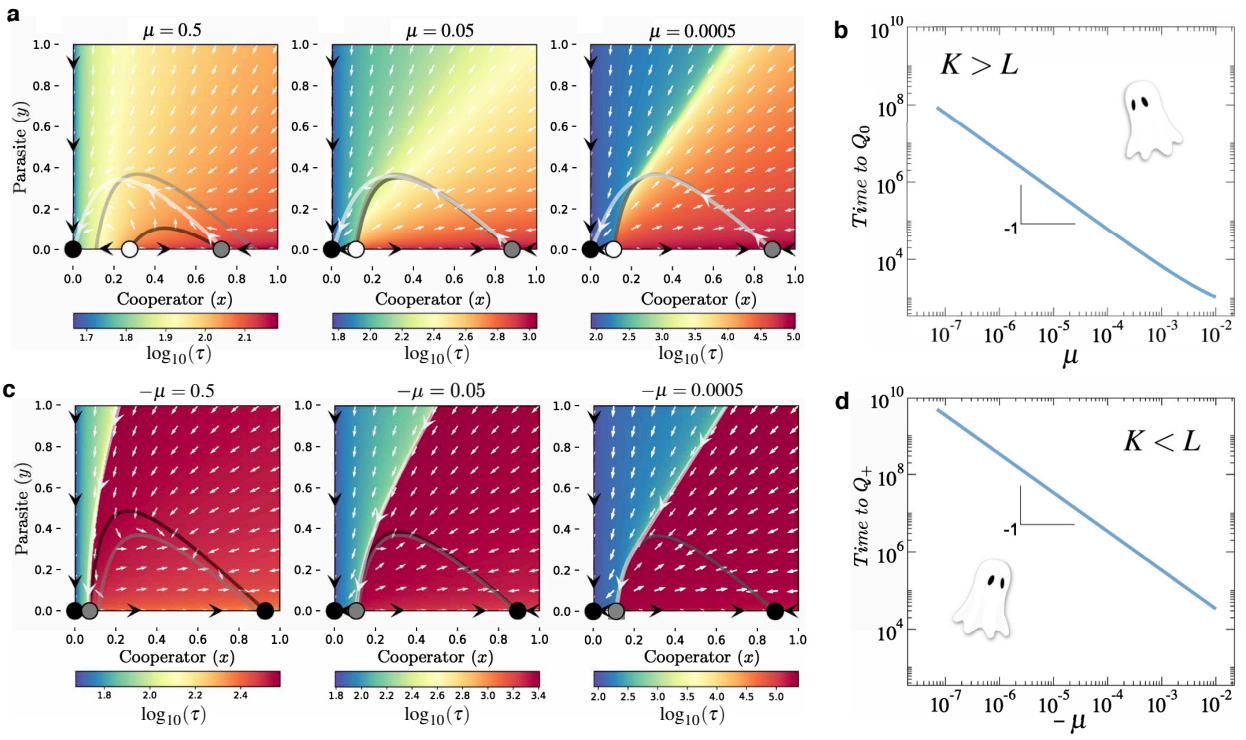

FIG. 3: Slowing down in the ghost CQNE close to the global bifurcation. (a) Time spent by the orbits to reach the co-extinction equilibrium for $\mu = 0.5$ (left), $\mu = 0.05$ (middle), and $\mu = 0.005$ (right). The nullclines (gray: $\mathscr{N}_h^2$; black:$\mathscr{N}_v^2$), the unstable manifold $\mathscr{W}_+^u$ (white) and the vector field (white arrows) are shown overlapped to the time colour map. Note that times largely increase as $\mu \to 0$. (b) Time to reach the co-extinction equilibrium, Q_0, as a function of the distance to the bifurcation value, which follows a scaling law of the form $\tau \sim |\mu|^{-1}$. (c) Same as in panel (a) at the other side of the bifurcation (case $\mu < 0$); the time spent to reach either the attractors Q_0 or Q_+ is represented. Here the white curve shows the stable manifold $\mathscr{W}_-^s$. Panel (d) displays the same scaling behaviour as in (b), now for the time spent to reach either Q_0 or the Q_+ attractor. In panels (b) and (d) we have set $x(0) = 1$ and $y(0) = 0.5$.

transients and the distance to the bifurcation value, here with $\tau \sim |\mu|^{-1}$; see Figure 3(b).

Figure 3(c) shows results obtained for the case $\mu \lesssim 0$. Here the times that different initial conditions spend to reach either the Q_0 or Q_+ attractor are also displayed in colour gradients. The delaying capacity of the ghost CQNE also occurs here, (approximately) within the basin of attraction of $\mathscr{Q}$ which existed for $\mu = 0$. Note that the relative position of the nullclines is inverted with respect to the case $\mu > 0$, and they get extremely close near bifurcation threshold. Interestingly, we have found the same scaling behaviour of transient times, given by $\tau \sim |\mu|^{-1}$. Although the scaling exponent stays the same above and below the global bifurcation, the length of the transients towards Q_+ is larger; which means that, close to the bifurcation, the stabilisation of the cooperative species at equilibrium might take longer. Some

illustrative examples of the dynamics for $\mu \lesssim 0$ are shown in Figure 5. As mentioned, the case $\mu \leq 0$ involves a bistable scenario and, depending on the initial condition, both co-extinction or outcompetition of the parasite can take place. Panel (a) displays a case far away from the bifurcation in which dynamics towards the two attractors are fast. The time series are displayed in panels (c) and (d) for different initial conditions. Figure 5(b,e) show the slow dynamics arising at $\mu = 5 \times 10^{-4}$. Here, those orbits within the basin of attraction of Q_0 travel very fast, but the initial conditions in the basin of attraction of Q_+ experience a ghost transient as passing the bottleneck region of the CQNE.

2. *Analytical derivation of the scaling laws*

Here we study the scaling law for the times to reach an attractor for system (5)–(6) in terms of the parameter μ which we assume to be small. First we consider the case $\mu > 0$ (case (a) below). The case $\mu < 0$ will be discussed in Section II C 2(b).

(a) Case $K > L$.

Let us first provide a description of the relative position of the nullclines in this case (see also Figure 2(a)). Recall that $\mathcal{N}_v^2$ and $\mathcal{N}_h^1$ are represented by $y = g_v(x)$ and $y = g_h(x)$ (see (9)), respectively. When $\mu > 0$, the zeros of g_v and g_h (see (10)) exist and are different if

$$\gamma < \frac{CL}{4}, \tag{18}$$

and satisfy $\xi_- < \delta_- < \delta_+ < \xi_+$. From now on, in the case $\mu > 0$, the condition (18) will be assumed to hold. We recall that the functions $g_v(x)$ and $g_h(x)$ reach an absolute maximum at $x = x_v$ and $x = x_h$, respectively (see (13)). Clearly, $g_h(x) > g_v(x)$ and $x_h < x_v$ for $\mu > 0$.

Lemma 1 provides information regarding the distance between the points in (10) and the value of the functions (11) and (12) on them in terms of μ. Its proof is deferred to Section II C 3.

Lemma 1 *Assume that $\mu > 0$ and $\gamma < CL/4$. Then, the terms $(\xi_+ - \delta_+)$ and $(\delta_- - \xi_-)$ are of order μ, whereas the terms $(\xi_+ - \delta_-)$ and $(\delta_+ - \xi_-)$ are of order μ^0. Moreover, $g_v(\xi_\pm)$ and $g_h(\delta_\pm)$ are of order μ.*

The positive invariance of the domain Σ and the location of the horizontal and the vertical nullclines (see Figure 6) makes the dynamics quite simple. Within these dynamics, we focus our attention on those orbits $(x(t), y(t))$ with initial conditions on the line $x + y = C$. From (5) it is clear that its x-variable is always decreasing. Furthermore, whenever these orbits are above $y = g_h(x)$, their y-variable is decreasing as well. This makes their ω-limit to be the origin or the point $Q_+ = (\xi_+, 0)$, the latter only if we start at the point $(C, 0)$.

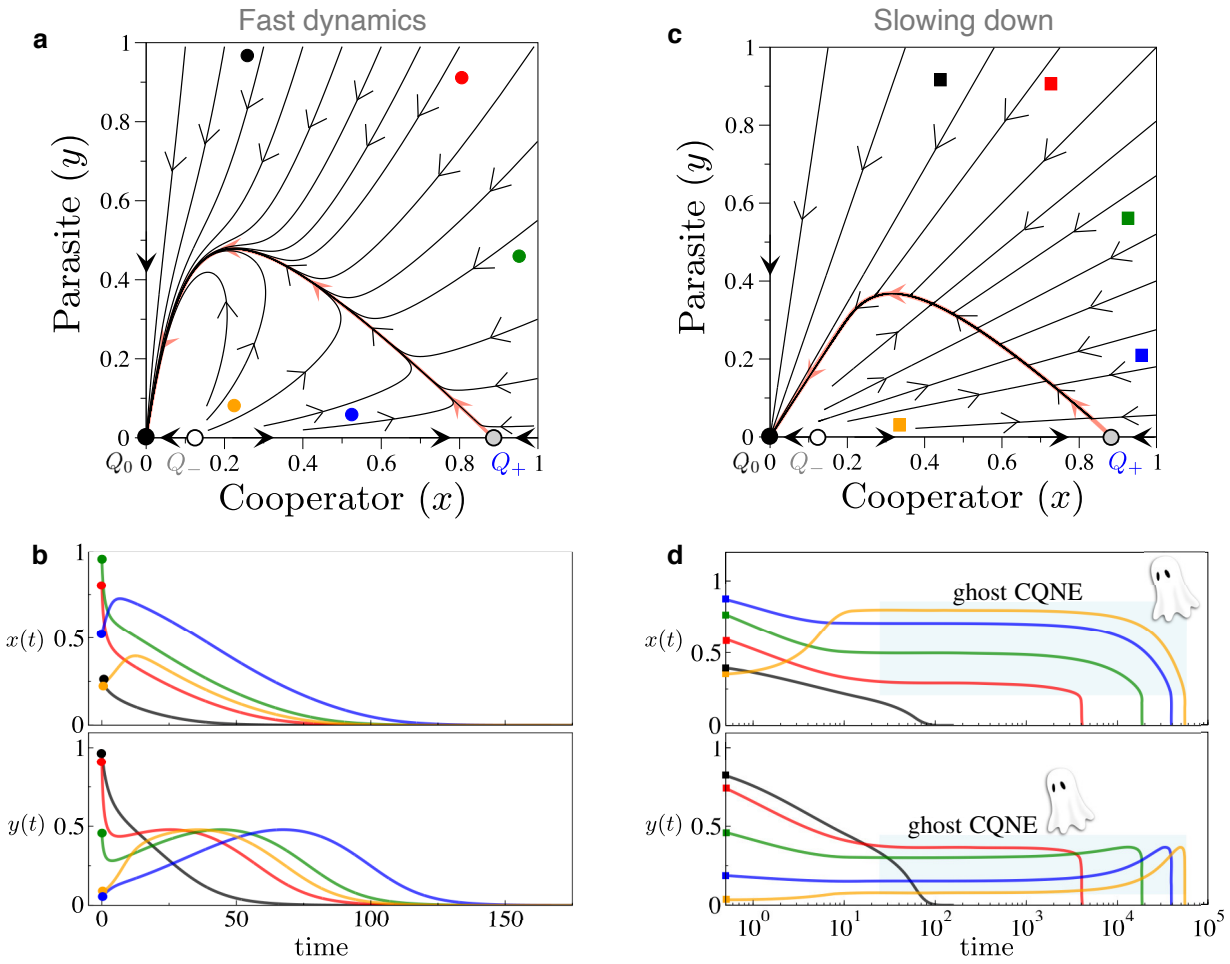

FIG. 4: Dynamics for the case $K > L$, involving a monostable scenario with extinction of cooperators and parasites. In (a) and (c) we display phase portraits setting $K = 1.5$ ($\mu = 0.5$) and $K = 1.0005$ ($\mu = 5 \times 10^{-4}$ close to the global bifurcation), respectively. (b) Transients to co-extinction with a value of K far from the bifurcation. The used initial conditions are the ones represented with the same colours and symbols in phase portrait (a). (d) Delayed extinctions close to the global bifurcation, using the initial conditions of phase portrait (c) indicated with small squares. Here the orbits rapidly reach the ghost Curve of Quasi-Neutral Equilibria (CQNE), then going very slowly to extinction. In all the simulations we have set $L = 1$ and $\gamma = 0.1$.

The dynamics of the solutions of (5)-(6) with initial conditions on $x+y=C$ present two different scenarios. This depends on whether they are located above or below the special solution $\mathscr{O}_{\tan}$ which, having initial condition at $(x_{\tan}, C-x_{\tan})$, intersects tangentially the horizontal nullcline $y = g_h(x)$ at the point $(x_h, g_h(x_h))$; see Figure 6. Hence, we can consider two scenarios:

- The orbits located on or above $\mathscr{O}_{\tan}$, which decay until they reach (in infinite time) the attractor at the origin. They do not cross the horizontal nullcline.

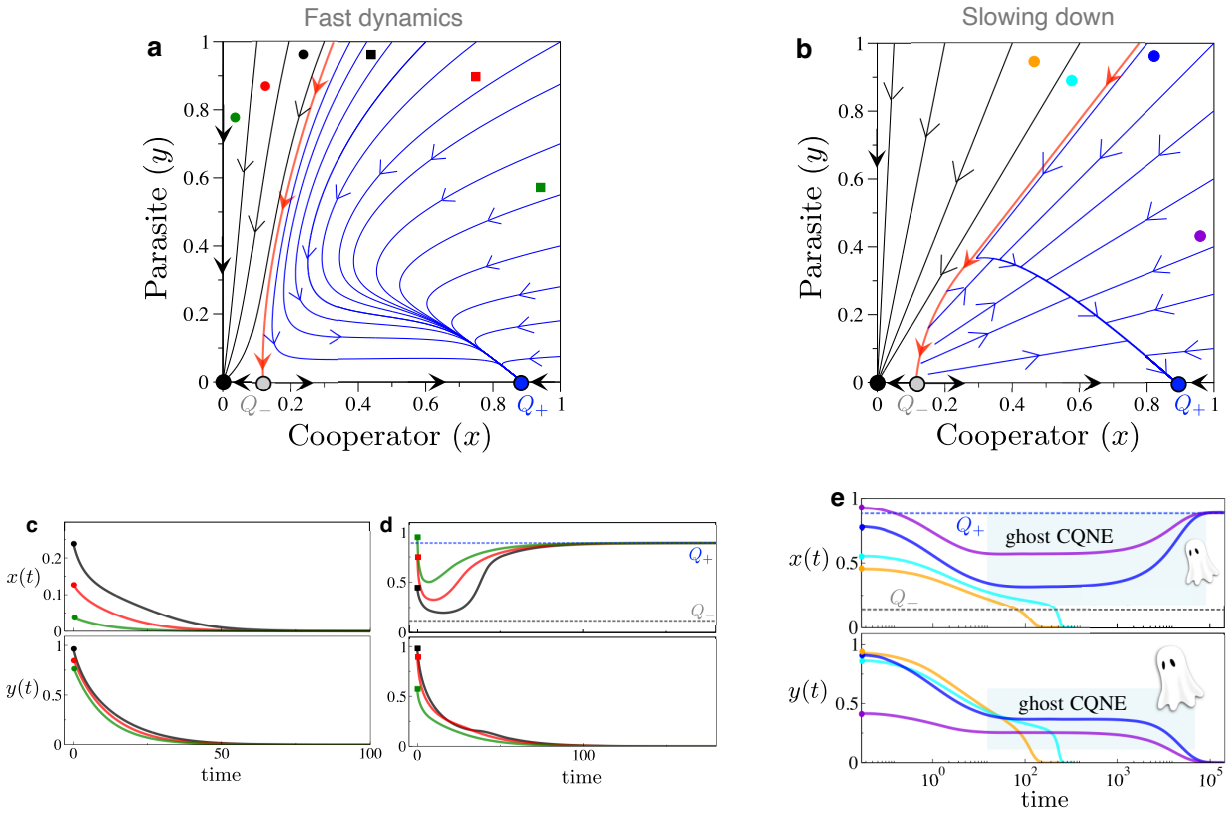

FIG. 5: Dynamics for the case $K < L$. Phase portraits with $K = 0.5$ ($\mu = -0.5$) (a), and $K = 0.9995$ ($\mu = -5 \times 10^{-4}$, close to the global bifurcation) (b). Black and blue orbits denote full extinction and only-parasites extinction, respectively. The small circles and squares correspond to initial conditions used in the time series below: (c) initial conditions in the basin of attraction of Q_0; (d) initial conditions in the basin of attraction of Q_+. Panel (e) displays the dynamics close to the global bifurcation. Notice that the blue and violet circle show initial conditions allowing the survival of the cooperator and a delayed extinction of the parasites, showing a long bottleneck given by the ghost Curve of Quasi-Neutral Equilibria (CQNE). In all cases we have set $L = 1$ and $\gamma = 0.1$.

- The orbits below $\mathscr{O}_{\tan}$, which decay until they meet $y = g_h(x)$, enter into the region D_2 and leave it to end (in infinite time) at the origin.

We restrict ourselves to the latter. To be more precise, we fix a small positive constant ρ and define the interval

$$I_\rho := [x_{\tan} + \rho, C - \rho]\,.$$

Definition 1 *We say that a solution of* (5)-(6) *belongs to the family* $\mathscr{F}_\rho$ *if its initial condition* $(x(0), y(0)) = (x_0, y_0)$ *satisfies* $x_0 + y_0 = C$ *with* $x_0 \in I_\rho$.

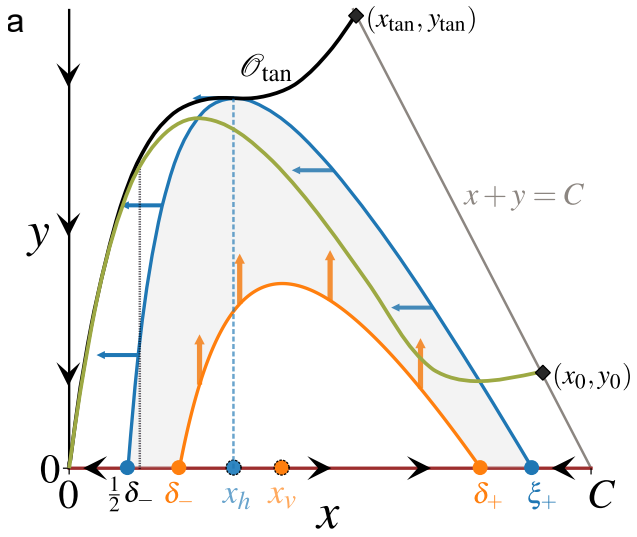

FIG. 6: Trajectories with initial conditions on $x+y=C$ that enter into D_2 (olive green colour curve) are bounded by the orbit $\mathscr{O}_{\tan}$ (black), which is tangent to the horizontal nullcline. The orbit starting at (x_0, y_0) the line $x=\delta_-$ (not shown) at time $t=\tau_1$, while τ_2 is the flight time from $x=\delta_-$ to $x=\frac{1}{2}\delta_-$.

Now, we consider an orbit $\mathscr{O} \in \mathscr{F}_\rho$ and define its flight time τ from its initial condition until it reaches the vertical line $x=\frac{1}{2}\delta_-$. We remark that $x=\frac{1}{2}\delta_-$ could be substituted by any value in $(0,\xi_-)$. Our aim is to provide lower and upper estimates for this time τ in terms of μ.

Theorem 1 *Given $\mathscr{O} \in \mathscr{F}_\rho$, let τ be the flight time until it reaches the line $x=\frac{1}{2}\delta_-$. Then, there exist constants $0<M_1<M_2$ and $\mu_0>0$, which depend on the parameters C,γ,L,x_0, but independent of μ, such that the following estimates hold:*

$$\frac{M_1}{\mu} < \tau < \frac{M_2}{\mu}, \qquad 0<\mu<\mu_0.$$

Before giving the proof, we introduce the following change of variables, which brings $\mathscr{N}_v^2$ to the line $z=0$:

$$\begin{pmatrix} x \\ z \end{pmatrix} = \Phi(x,y) := \begin{pmatrix} x \\ y - g_v(x) \end{pmatrix}. \tag{19}$$

In the new variables, system (5)-(6) becomes

$$\begin{aligned} \dot{x} &= -\frac{L}{C}x^2 z, \\ \dot{z} &= a(x)z^2 + b(x)z + c(x), \end{aligned} \tag{20}$$

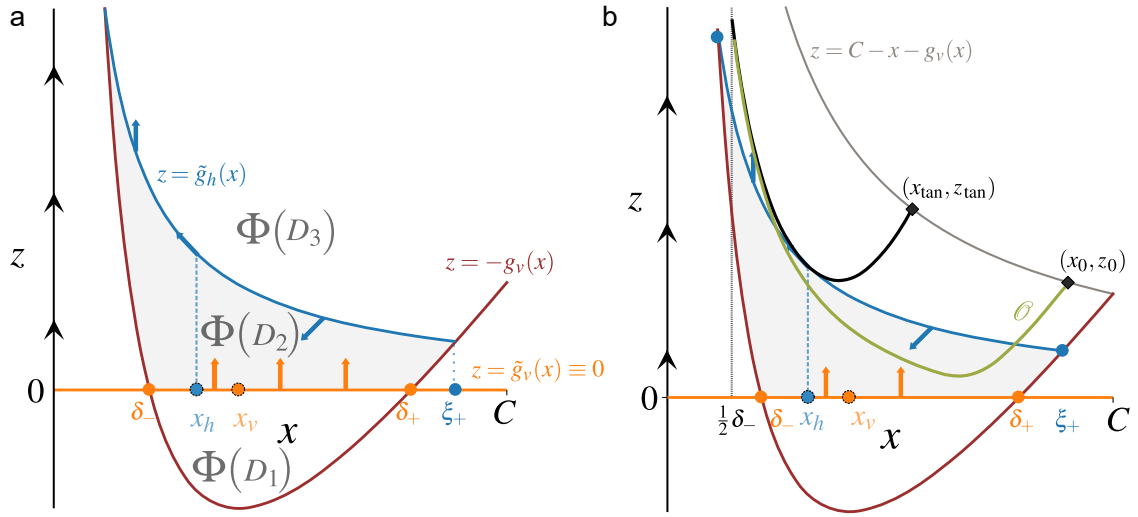

FIG. 7: Transformation of curves and domains by means of the change of variables $z = y - g_v(x)$, see (19). In (a), transformation of the Figure 2; in (b), the construction of Figure 6 in the new variables.

where

$$\begin{aligned} a(x) &= -\frac{K}{C}x = -\frac{x}{C}\mu - \frac{L}{C}x, \\ b(x) &= 2\frac{\gamma K}{L} - Kx + \frac{(K-L)}{C}x^2 = \mu\left(\frac{2\gamma}{L} + \frac{x^2}{C} - x\right) + 2\gamma - Lx, \\ c(x) &= \frac{\gamma}{L}g_v(x)\,\mu. \end{aligned} \tag{21}$$

After this change of variables, the relevant curves of the system are transformed as follows:

- $y = g_v(x)$ becomes $z = 0$ (sometimes referred to as $\tilde{g}_v(x) \equiv 0$);
- $y = g_h(x)$ becomes $z := \tilde{g}_h(x) = g_h(x) - g_v(x) = \dfrac{\gamma C}{KL}\dfrac{1}{x}\mu$;
- $y = 0$ becomes $z = -g_v(x)$;
- $y = C - x$ becomes $z = C - x - g_v(x)$.

Figure 7 shows the transformed domains. Since $y > 0$ for the solutions in $\mathscr{F}_\rho$, the dynamics stays above the thick black curve in Figure 7. Note that $z = -g_v(x)$ and $z = \tilde{g}_h(x)$ intersect at $x = \xi_\pm$. Moreover, since $y < C - x$ in D_2, the dynamics holds below $z = C - x - g_v(x)$. In the new coordinates (x,z) we will also use the symbol $\mathscr{F}_\rho$ to refer to the orbits with initial conditions (x_0,z_0) on $z = C - x - g_v(x)$ with $x_0 \in I_\rho$. The proof of Theorem 1 depends on the results of Section II C 3.

Proof. [**Theorem 1**] For the lower bound it is enough to get one for a smaller time. Actually, we will look for a lower bound for the time τ_ℓ needed to go from $x = x_2$ to $x = x_h$, where (x_2,z_2) is the point where the

orbit $\mathscr{O}$ (green curve in panel (b) of Figure 7) enters $\Phi(D_2)$, that is, $z_2 = \tilde{g}_h(x_2)$ (see the intersection of green and blue curves in panel (b) of Figure 7). In this interval of time, the orbit is in $\Phi(D_2)$ and then $z < \tilde{g}_h(x)$.

Hence, from the first equation of system (20) and the definition of $\tilde{g}_h(x)$, we have

$$\dot{x} = -\frac{L}{C}x^2 z > -\frac{L}{C}x^2\,\tilde{g}_h(x) = -x\,\frac{\gamma}{K}\mu.$$

Therefore,

$$\frac{\dot{x}}{x} > -\frac{\gamma}{K}\mu \quad \Longrightarrow \left[\log x\right]_{x_2}^{x_h} > -\frac{\gamma}{K}\mu\,\tau_\ell,$$

and

$$\tau_\ell > \frac{L+\mu}{\gamma\mu}\log\frac{x_2}{x_h}. \tag{22}$$

Since $x_0 \geq x_{\tan} + \rho$, when $\mu = 0$ the orbit with initial condition (x_0, z_0) arrives to the curve $z = \tilde{g}_h(x)$ at some point (x_1, z_1) with $x_1 > x_h$. Then, the orbit corresponding to this value of μ will arrive at some point $x_2 = x_1 + O(\mu)$ and therefore, if μ is small enough, $x_2 - x_h > m_1 > 0$, with m_1 independent of μ. Then, there exists $M_1 > 0$ independent of μ such that

$$\tau > \tau_\ell > M_1/\mu.$$

For the upper bound we divide τ into two parts, τ_1 and τ_2 (see Figure 6):

- $\tau_1 \geq 0$ is the time spent from the initial condition (x_0, y_0) to reach the line $x = \delta_-$, i.e., $x(\tau_1) = \delta_-$.
- τ_2 is the time spent to go from $x = \delta_-$ to $x = \frac{1}{2}\delta_-$.

(i) **Upper bound for τ_1.** From Proposition 1, for $x = x(t) \in [\delta_-, x_0]$, it follows that

$$\dot{x} = -\frac{K}{C}x^2 z < -\frac{K}{C}M_3\mu x^2 \Rightarrow \frac{\dot{x}}{x^2} < -\frac{K}{C}M_3\mu.$$

Therefore,

$$\tau_1 < -\frac{C}{KM_3}\,\frac{1}{\mu}\int_{x_0}^{\delta_-}\frac{dx}{x^2} = -\frac{C}{KM_3}\,\frac{1}{\mu}\left[-\frac{1}{x}\right]_{x_0}^{\delta_-} < \frac{C}{LM_3}\left(\frac{1}{\delta_-} - \frac{1}{x_0}\right)\frac{1}{\mu}.$$

(ii) **Upper bound for τ_2.** Let us consider for a while the original variables (x, y). Since $\dot{y}(t) > 0$ in D_2 it follows that $\mathscr{O}$ must leave it through the arc of $y = g_h(x)$ determined by the points $(x_h, g_h(x_h))$ and $(x_3, y_3) = (x_v(1 - \sqrt{\mu/K}), g_v(x_v))$, the latter being the point where $y = g_h(x)$ intersects the line $y = g_v(x_v)$. Since $\delta_- < x_v$, from the previous expression for x_3, it follows that $\delta_- < x_3 < x_v$ for small

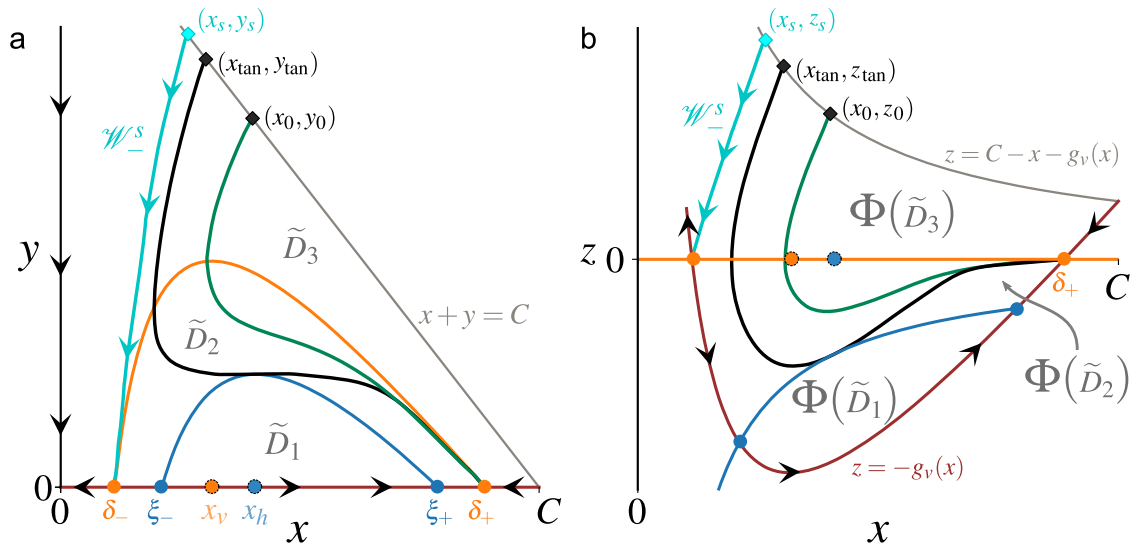

FIG. 8: Case $K < L$. Representative orbits (a) on the (x,y)-plane and (b) on the (x,z)-plane.

enough μ. Since the orbit $\mathscr{O}$ cannot reenter D_2 once it has leaved it, we have that $y(t) > g_h(x(t))$ if $0 < x(t) < \delta_-$. Therefore,

$$z > g_h(x) - g_v(x) = \tilde{g}_h(x) = \frac{\gamma C}{KL}\frac{1}{x}\mu.$$

As a consequence, $\dot{x} = -\dfrac{L}{C}x^2 z < -\dfrac{\gamma}{K}x\mu$. Since $x > 0$, this implies that

$$\frac{\dot{x}}{x} < -\frac{\gamma}{K}\mu$$

and so

$$\Big[\log x\Big]_{\delta_-}^{\frac{\delta_-}{2}} < -\frac{\gamma}{K}\mu\,\tau_2 \quad \Longrightarrow \quad \tau_2 < \left(\frac{L+\mu_0}{\gamma}\log 2\right)\frac{1}{\mu}.$$

The assertion of the theorem follows if we take

$$M_2 := \frac{C}{LM_3}\left(\frac{1}{\delta_-} - \frac{1}{x_0}\right) + \left(\frac{L+\mu_0}{\gamma}\log 2\right).$$

□

(b) Case $K < L$. We now consider the case $K < L$ and we show that the transient times also scale as $|\mu|^{-1}$, where $\mu = K - L$. In this case, $\mathscr{N}_v^2$ and $\mathscr{N}_h^2$ invert their relative position compared with the case $\mu > 0$ as it can be checked in Figures 2(b) and 8(a).

We will keep the notation used in the case $\mu > 0$; here, in order to have the maximum of $\mathscr{N}_h^2$ above the x axis, we need to assume that $\gamma < CK/4$ (however, recall that $K = L + \mu$). We recall that for $\mu < 0$,

we have that $Q_- = (\delta_-, 0)$ is a saddle point and $Q_+ = (\delta_+, 0)$ is an attracting node. As for $\mu > 0$, $(0,0)$ is an attractor. The stable manifold of Q_-, $\mathscr{W}^s_-$ (see Figure 2 and Section II B), plays an important role since it separates the basins of attraction of both attractors. From $0 < g_v'(\delta_-) < m_-$ (see (17) in Section II B), we deduced that the upper local part of $\mathscr{W}^s_-$ near Q_- stays in $\widetilde{D}_3$. Since it is (a piece of) an orbit $\mathscr{O}$, its globalization (for negative time) cannot intersect neither $\{x = 0\}$ nor $\{y = 0\}$ nor the graph of g_v. Then, either it stays in $\widetilde{D}_3$ forever or it arrives to the upper boundary $\{x + y = C\}$ of $\widetilde{D}_3$. Since in $\widetilde{D}_3$, $\dot{x} < 0$ and $\dot{y} < 0$, we have that both $x(t)$ and $y(t)$ are strictly monotonically decreasing. Therefore, if $\mathscr{O}$ stays in $\widetilde{D}_3$ for negative time, it has to converge (for negative time) to some equilibrium point. Clearly, it cannot converge to $(0,0)$ nor to Q_- and, hence, it must arrive, in finite time, at some point on $\{x + y = C\}$, that we call (x_s, y_s), where $y_s = C - x_s$ (see Figure 8(a)).

Given $\rho > 0$, we consider the interval

$$J_\rho := [x_s + \rho, C - \rho].$$

Definition 2 *We say that a semiorbit $\mathscr{O}$ belongs to the family $\widetilde{\mathscr{F}_\rho}$ if $x(0) + y(0) = C$ and $x(0) \in J_\rho$.*

Clearly, if $\mathscr{O} \in \widetilde{\mathscr{F}_\rho}$, it starts in $\widetilde{D}_3$, where $\dot{x} < 0$ and $\dot{y} < 0$. It cannot cross $\mathscr{W}^s_-$. Then, it must converge to the ω-limit set Q_+.

On the other hand, since $\lambda_+^{(1)}$ does not depend on μ, when K is close enough to L, $|\lambda_+^{(2)}| < |\lambda_+^{(1)}|$, which means that there is a slow manifold of Q_+ tangent to $(1, m_+)$. Consequently, when the orbits approach Q_+, they arrive tangent to the direction $(1, m_+)$, except for the strong stable manifold, which is contained in $y = 0$. Due to the relation between the slopes, this fact implies that for all orbits tending to Q_+, except for the strong stable manifold, there exists a time t_c such that the orbit is contained in $\widehat{D}_2 \subset \widetilde{D}_2$ for all $t > t_c$, where

$$\widehat{D}_2 := \{(x,y) \in \Sigma \,|\, x_h < x < \delta_+, g_h(x) < y < g_v(x)\},$$

see Figure 9.

Since Q_+ is an attractor, any solution that converges to it spends infinite time to reach it. Therefore, we choose $\eta > 0$ small but fixed, independent of all parameters, and we estimate the time needed to arrive to $\{x = \delta_+ - \eta\} \cap \widetilde{D}_2$.

Theorem 2 *Consider $\rho > 0$, $\eta > 0$ and the solution $(x(t), y(t))$ of (5)–(6) with initial condition (x_0, y_0) with $x_0 \in J_\rho$ and $y_0 = C - x_0$. Let τ be such that $x(\tau) = \delta_+ - \eta$. Then, there exist positive constants M_4, M_5*

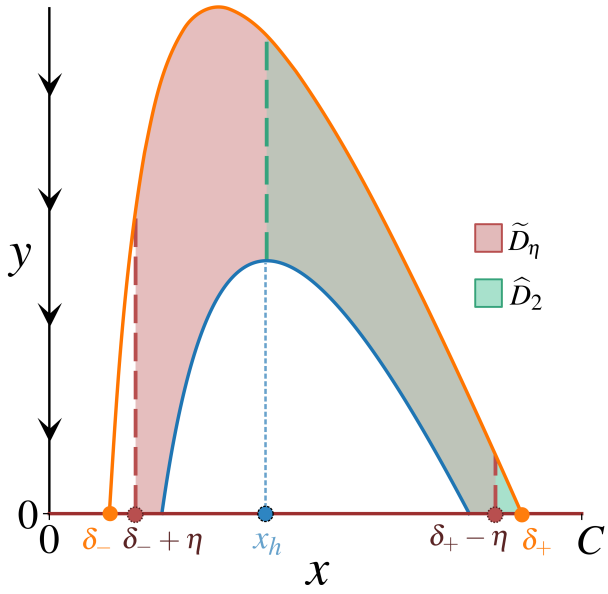

FIG. 9: Nullclines of the transformed system (x,z) for $K < L$. The region coloured in pink is $\widetilde{D}_\eta$; in turquoise, the region $\widehat{D}_2$; the region in grey is $\widetilde{D}_\eta \cap \widehat{D}_2$. For the sake of clarity of the plot, we have chosen parameters far from the bifurcation, more specifically, $L = 0.6$, $K = 1.0$, and $\gamma = 0.05$.

and μ_0 such that

$$\frac{M_4}{|\mu|} \le \tau \le \frac{M_5}{|\mu|} \qquad \text{for } |\mu| < \mu_0.$$

We first check that the modulus of the vector field, $\|F(x,y)\|$, is bounded linearly in $|\mu|$.

Lemma 2 *Let $\eta > 0$ be small and consider $\widetilde{D}_\eta = \{(x,y) \in \Sigma |\ \delta_- + \eta < x < \delta_+ - \eta, g_h(x) < y < g_v(x)\}$. Then, there exist two positive constants $m_\ell = m_\ell(C,L,\gamma)$ and $m_u = m_u(C,L,\gamma)$ such that*

$$m_\ell |\mu| \le \|F(x,y)\| \le m_u |\mu|$$

for $(x,y) \in \widetilde{D}_\eta$.

Proof. [**Theorem 2**]

Consider a piece of solution $\varphi(t) = (x(t), y(t))$ of (5)–(6) contained in $\widetilde{D}_\eta$, $0 < t_c \le t \le \tau$. Then, for any $t \in [t_c, \tau]$,

$$\|\varphi(t) - \varphi(t_c)\| = \left\| \int_{t_c}^{t} \dot{\varphi}(s)\, ds \right\| \le \int_{t_c}^{t} \|\dot{\varphi}(s)\|\, ds = \int_{t_c}^{t} \|F(\varphi(s))\|\, ds \le m_u |\mu| (t - t_c),$$

which gives the following lower bound for the time to go from $\varphi(t_c)$ to $\varphi(\tau)$:

$$\tau > \tau - t_c \ge \frac{\|\varphi(\tau) - \varphi(t_c)\|}{m_u} |\mu|^{-1} =: M_4 |\mu|^{-1}. \tag{23}$$

Moreover, since $\dot{x} > 0$ and $\dot{y} < 0$ in $\widehat{D}_2$, we have an equality in the above triangle inequality:

$$\left\| \int_{t_c}^{t} \dot{\varphi}(s)\, ds \right\| = \int_{t_c}^{t} \|\dot{\varphi}(s)\|\, ds = \int_{t_c}^{t} \|F(\varphi(s))\|\, ds \geq m_\ell\, |\mu|\, (t - t_c),$$

and then

$$\tau - t_c \leq \frac{\|\varphi(\tau) - \varphi(t_c)\|}{m_\ell} |\mu|^{-1} =: M_5 |\mu|^{-1}. \tag{24}$$

The latter bound is for the part of the orbit inside $\widehat{D}_2$, but the time spent outside is bounded independently of μ and so, the transient time is asymptotically of order $|\mu|^{-1}$. The result follows because $x(\tau) = \delta_+ - \eta$ and $x(t_c)$ depends on the initial conditions and it is of the form $a + O(\mu)$ with $a < \delta_+$.

□

Proof. [**Lemma 2**] We follow the notation in (7)–(8): $F(x,y) = (F_1(x,y), F_2(x,y)) = (Lx^2\,(g_v(x) - y)/C, Kxy\,(g_h(x) - y)/C)$. Using that in $\widehat{D}_2$, $F_1(x,y) > 0$, $F_2(x,y) < 0$,

$$F_1(x,y) < F_1(x, g_h(x)) < \frac{L}{C} x^2 (g_v(x) - g_h(x)) = \gamma x \left(\frac{L}{K} - 1 \right),$$

and

$$F_2(x,y) > F_2(x, g_v(x)) > \frac{K}{C} xy (g_h(x) - g_v(x)) = \gamma y \left(\frac{K}{L} - 1 \right),$$

we have

$$\|F(x,y)\|^2 \leq \gamma^2 x^2 \frac{(L-K)^2}{K^2} + \gamma^2 y^2 \frac{(L-K)^2}{L^2} \leq \frac{\gamma^2}{K^2} (x^2 + y^2) \mu^2,$$

and therefore there exists a m_{u}, independent of μ, such that

$$\|F(x,y)\| \leq m_{\mathrm{u}} |\mu|.$$

For the lower bound, we first change the variables (x,y) to $\zeta = (x,z)$ as in (19); in the transformation of $\widehat{D}_2$ by (19), we have $\dot{\zeta} = \widetilde{F}(\zeta)$, where

$$\widetilde{F}(x,z) = \left(-\frac{L}{C} x^2 z, a(x) z^2 + b(x) z + c(x) \right),$$

as defined in (20). Therefore, since $a(x)\, c(x) > 0$ for $\mu < 0$,

$$\begin{aligned} \left\| \widetilde{F}(\zeta) \right\|^2 &= (-\frac{L}{C} x^2 z)^2 + (a(x) z^2 + b(x) z + c(x))^2 \geq \frac{L^2}{C^2} x^4 z^2 + (b(x) z + c(x))^2 - |2a(x) b(x) z^3| \\ &\geq \frac{L^2}{C^2} x^4 z^2 + (b(x) z + c(x))^2 - M_7 |\mu|^3, \end{aligned}$$

where we have used that the upper bound $|z| < |\tilde{g}_h(\delta_- + \eta)| < \frac{C}{K}|\mu|$ and conveniently defined

$$M_7 := \left(\frac{C}{K}\right)^3 \max_{x\in\hat{J}_\eta}\{|2a(x)b(x)|\},$$

where $\hat{J}_\eta = [\delta_- + \eta, \delta_+ - \eta]$.

Next, we estimate the term $\dfrac{L^2}{C^2}x^4 z^2 + (b(x)z + c(x))^2$ for $(x,z) \in \Phi(\widehat{D}_2)$, which we write as

$$\beta(z;x) := \alpha(x)^2 z^2 + (b(x)z + c(x))^2, \qquad \text{with } \alpha(x) := \frac{L}{C}x^2.$$

We look for the minimum of $\beta(z;x)$ in $z \in [\tilde{g}_h(x), 0]$ for x fixed in $\hat{J}_\eta$. Differentiating with respect to z and equating to 0, we get

$$\frac{d\beta}{dz} = 2\,\alpha(x)^2 z + 2\,(b(x)z + c(x))\,b(x) = 0 \qquad \Leftrightarrow \qquad z = z^* := -\frac{b(x)\,c(x)}{\alpha(x)^2 + b(x)^2}.$$

Clearly $\frac{d^2\beta}{dz^2} = 2\left(\alpha(x)^2 + b(x)^2\right) > 0$ and so β reaches a local minimum at z^* whose value is

$$\beta(z^*) \;= \frac{\alpha(x)^2 c(x)^2}{\alpha(x)^2 + b(x)^2} > M_8\,\mu^2,$$

for some $M_8 > 0$, independent of μ. Therefore,

$$\left\|\widetilde{F}(\zeta)\right\|^2 \geq M_8\,\mu^2 - M_7\,|\mu|^3,$$

and so, if μ is small enough, $\left\|\widetilde{F}(\zeta)\right\| \geq M_9|\mu|$, for some $M_9 > 0$.

Finally, in terms of the change of variables introduced in (19), Φ (so that $(x,z) = \Phi(x,y) = (x, y - g_v(x))$), we can write

$$F(x,y) = D\Phi^{-1}(\Phi(x,y))\,\widetilde{F}(\Phi(x,y))$$

and

$$\|F(x,y)\| \geq \left\|\left[D\Phi^{-1}(\Phi(x,y))\right]^{-1}\right\|^{-1} \left\|\widetilde{F}(\Phi(x,y))\right\|.$$

Since

$$\left[D\Phi^{-1}(\Phi(x,y))\right]^{-1} = D\Phi(x,y) = \begin{pmatrix} 1 & 0 \\ -g_v'(x) & 1 \end{pmatrix}$$

and, for $x \in \hat{J}_\eta$, its norm is bounded independently of μ for some constant M_{10}, then

$$\|F(x,y)\| \geq \frac{M_9}{M_{10}}\,|\mu| =: m_\ell\,|\mu|.$$

□

Proof of Lemma 1

Proof. We define $\Delta(x) := \sqrt{C^2 - 4\gamma C/x}$. Then,

$$\xi_+ - \delta_+ = \frac{1}{2}\left(\Delta(K) - \Delta(L)\right) = \frac{2\gamma C}{K_0^2 \Delta(K_0)}\mu, \qquad \text{with } K_0 \in (L,K),$$

where we have applied the Mean Value Theorem to $\Delta(x)$. Note that $\xi_+ - \delta_+ = \dfrac{2\gamma C}{L^2\Delta(L)}\mu + O(\mu^2)$. Besides, since $\xi_+ - \delta_- = (\xi_+ - \delta_+) + (\delta_+ - \delta_-)$ and $\delta_+ - \delta_- = \Delta(L) = O(\mu^0)$, we have that $\xi_+ - \delta_- = \Delta(L) + O(\mu) = O(\mu^0)$. The claims for $\delta_- - \xi_-$ and $\delta_+ - \xi_-$ follow from $\delta_- - \xi_- = \xi_+ - \delta_+$ and $\delta_+ - \xi_- = \xi_+ - \delta_-$.

Finally, we consider $g_v(\xi_+)$ (a similar proof works for $g_h(\delta_+)$, $g_v(\delta_-)$ and $g_h(\xi_-)$). Expanding g_v around δ_+ one gets

$$g_v(\xi_+) = g_v(\delta_+) + g_v'(\delta_+)(\xi_+ - \delta_+) + O\left((\xi_+ - \delta_+)^2\right) = \left(-2 + \frac{C}{\delta_+}\right)(\xi_+ - \delta_+) + O\left((\xi_+ - \delta_+)^2\right) = O(\mu).$$

□

Let x_b be

$$x_b = \frac{2\gamma}{L}, \tag{25}$$

which satisfies that $b_{|_{\mu=0}}(x_b) = 0$, where $b(x)$ is introduced in (21).

Lemma 3 *If $\gamma < CL/4$, then we have that*

$$\delta_- < x_b < \delta_+. \tag{26}$$

Proof.

$$x_b > \delta_- \Leftrightarrow \frac{2\gamma}{L} > \frac{C - \sqrt{C^2 - 4\gamma C/L}}{2} \Leftrightarrow \sqrt{C^2 - 4\gamma C/L} > C - \frac{4\gamma}{L} \Leftrightarrow C^2 - \frac{4\gamma C}{L} > C^2 + \frac{16\gamma^2}{L^2} - \frac{8\gamma C}{L} \Leftrightarrow C > \frac{4\gamma}{L},$$

which is true by hypothesis. Also, from the definition of δ_+ it is clear that

$$\delta_+ > \frac{C}{2} > \frac{1}{2}\frac{4\gamma}{L} = x_b.$$

□

Remark 1 *Note that all terms in (26) are independent of μ.*

Lemma 4 *Let $\mu > 0$. Then, the following assertions hold:*

a) The horizontal nullcline $\dot{z} = 0$ of system (20) (see Figure 10) is the union of two disjoint curves, $z = z_\pm(x)$. They satisfy that $z_+(x) > 0$ and $z_-(x) < 0$ for $x \in (\delta_-, \delta_+)$.

b) There exists a constant $M_{11} > 0$, independent of μ, such that

$$z_+(x) > M_{11} g_v(x)\, \mu \qquad \forall x \in (\delta_-, \delta_+). \tag{27}$$

Moreover, there exist $M_6 > 0$ and $x_c \in (\delta_-, \delta_+)$, both independent of μ, such that

$$z_+(x) > M_6 \qquad \forall x \in [\delta_-, x_c].$$

Proof.

a) The horizontal nullcline is determined by

$$a(x)\, z^2 + b(x)\, z + c(x) = 0, \tag{28}$$

with $a(x)$, $b(x)$ and $c(x)$ defined in (21). The solutions of this equation are

$$z_\pm(x) = \frac{-b(x) \mp \sqrt{b(x)^2 - 4\, a(x)\, c(x)}}{2\, a(x)} = \frac{2\, c(x)}{-b(x) \pm \sqrt{b(x)^2 - 4\, a(x)\, c(x)}}. \tag{29}$$

For $x \in (\delta_-, \delta_+)$, we have that $a(x) = -\frac{K}{C} x < 0$ and $c(x) = \frac{\gamma}{L} g_v(x) \mu > 0$. Therefore, we have that $z_+(x) > 0$ for $x \in (\delta_-, \delta_+)$. Since $z_+(x) z_-(x) = c(x)/a(x) < 0$ for $x \in (\delta_-, \delta_+)$ it follows that $z_-(x) < 0$ in (δ_-, δ_+).

b) Note that $-b(x) + \sqrt{b(x)^2 - 4\, a(x)\, c(x)}$ is bounded from above in $[\delta_-, \delta_+]$ by a positive constant M_{12} depending on C, L and γ, provided μ is bounded. Therefore, from (29), we get equation (27):

$$z_+(x) > \frac{2\,\gamma}{L M_{12}} g_v(x)\, \mu =: M_{11} g_v(x)\, \mu,$$

as claimed. Regarding the second assertion, take $x_c = \frac{1}{2}(\delta_- + x_b)$, where x_b is defined in (25). From the definition of $z_+(x)$, that $a(x) < 0$, and the fact that μ is small, it follows for $x \in [\delta_-, x_c]$ that

$$\begin{aligned} z_+(x) &= \frac{-b(x) - \sqrt{b(x)^2 - 4a(x)c(x)}}{2a(x)} > -\frac{b(x)}{2a(x)} > \frac{2\gamma - Lx}{\frac{2Lx}{C}} + O(\mu) \\ &= \left(\frac{2\gamma}{Lx} - 1\right)\frac{C}{2} + O(\mu) > \left(\frac{x_b}{x_c} - 1\right)\frac{C}{2} + O(\mu). \end{aligned}$$

Then, there exists M_6 such that $z_+(x) > M_6$.

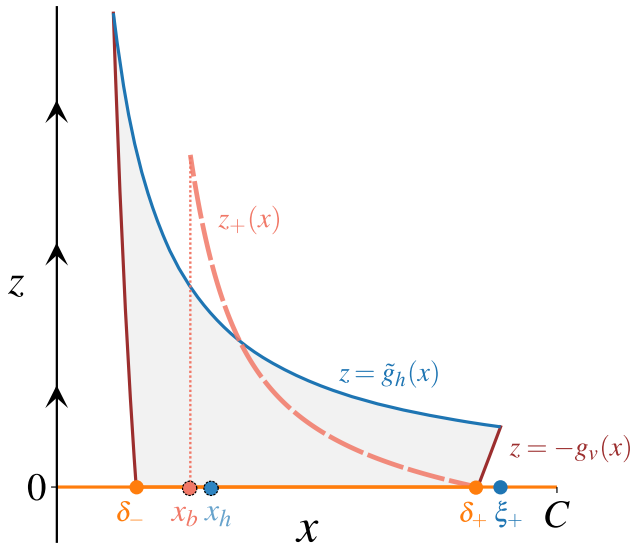

FIG. 10: Positive branch, $z=z_+(x)$ of the horizontal nullcline $\dot{z}=0$ of system (20). In fact, the z-nullcline is the union of two disjoint curves, $z=z_\pm(x)$. Only the positive branch has implications to determine the time bounds of the orbits we are interested in.

□

The following lemma ensures that the absolute minimum of $z(t)$, while $x(t)\in[\delta_-,x_0]$, must be reached in the interval (δ_-,δ_+).

Lemma 5 *Let $\mu>0$ and $\mathscr{O}=\{(x(t),z(t))\,|\,t\in\mathbb{R}^+\}\in\mathscr{F}_\rho$. Then, the following assertions hold:*

(a) If $x(t)=\delta_-$, then $\dot{z}(t)>0$.

(b) If $x(t)\geq\delta_+$, then $\dot{z}(t)<0$.

Proof.

(a) Assume that $x(t_1)=\delta_-$ for a given t_1. Using that $g_v(\delta_-)=0$, that $y(t_1)\leq g_h(x_h)=C-2\sqrt{\gamma C/K}=:M_{13}$, and having in mind that $z:=y-g_v(x)$, we have

$$z(t_1)\leq M_{13}-g_v(x(t_1))=M_{13}-g_v(\delta_-)=M_{13}.$$

Then,

$$\begin{aligned}\dot{z}(t_1) \;&>\; -\frac{K}{C}\delta_- z(t_1)^2+\left(\frac{2\gamma K}{L}-K\delta_-\right)z(t_1)=z(t_1)\left(-\frac{K}{C}\delta_- z(t_1)+\frac{2\gamma K}{L}-K\delta_-\right)\\ &\geq z(t_1)\left(\frac{2\gamma K}{L}-2\delta_-(K-\sqrt{\gamma K/C})\right)=\gamma z(t_1)\,\phi(\gamma),\end{aligned}$$

where

$$\phi(\gamma) = \frac{2K}{L} + \frac{4C/L}{C + \sqrt{C^2 - 4\gamma C/L}} \left(\sqrt{\frac{\gamma K}{C}} - K \right).$$

Since $\phi(0) = \frac{2K}{L} + \frac{4C/L}{2C}(-K) = 0$ and $\phi(\gamma)$ is strictly increasing with respect to γ, $\phi(\gamma) > 0$ for $\gamma > 0$. Summing up, $\dot{z}(t_1) > \gamma z(t_1)\,\phi(\gamma) > 0$ for $\gamma > 0$.

(b) Notice that $a(x) < 0$ and $c(x) \leq 0$ for $x \in [\delta_+, C - \rho]$. So, if $x(t) \geq \delta_+$ then

$$\begin{aligned} \dot{z}(t) &= a(x(t))z^2(t) + b(x(t))z(t) + c(x(t)) < b(x(t))z(t) = \big((2\gamma - Lx(t)) + O(\mu) \big) z(t) \\ &= \big(L(x_b - x(t)) + O(\mu) \big) z(t) < 0, \end{aligned}$$

since $x_b < \delta_+ \leq x(t)$ and μ small.

□

The next proposition proves the existence of a lower bound of order μ for the z-component of any orbit in $\mathscr{F}_\rho$.

Proposition 1 *Let $\mu > 0$ and $\mathscr{O} = \{(x(t), z(t)) \mid t \in \mathbb{R}^+\} \in \mathscr{F}_\rho$. Then, there exists a constant $M_3 > 0$, depending on x_0, γ, C, and L, but independent of μ, such that*

$$z(t) > M_3 \mu \qquad \text{if} \quad x(t) \in [\delta_-, x_0]. \tag{30}$$

Proof. First, observe that, if $x_0 > \delta_+$, then $z(t_3) > 0$, where t_3 is such that $x(t_3) = \delta_+$.

We next prove that $z(t) > z(t_3)$ for $0 \leq t < t_3$, i.e. when $x(t) \in (\delta_+, x_0]$, for μ small enough. Indeed, if $x(t) \in (\delta_+, x_0]$ we have

$$c(x(t)) = \frac{\gamma}{L} g_v(x(t))\mu < 0, \qquad a(x(t)) = -\frac{K}{C} x(t) < 0.$$

Moreover, since $x_b < \delta_+ < x(t)$, it follows that

$$b_{|\mu=0}(x(t)) = L(x_b - x(t)) < 0$$

and, consequently,

$$b(x) = \mu \left(\frac{2\gamma}{L} + \frac{x^2(t)}{C} - x(t) \right) + L(x_b - x(t)) < 0,$$

for μ small enough, which implies that, provided $x(t) \in (\delta_+, x_0]$,

$$\dot{z}(t) = a(x)z^2(t) + b(x)z(t) + c(x) < 0 \qquad \Rightarrow \qquad z(t) > z(t_3) > 0.$$

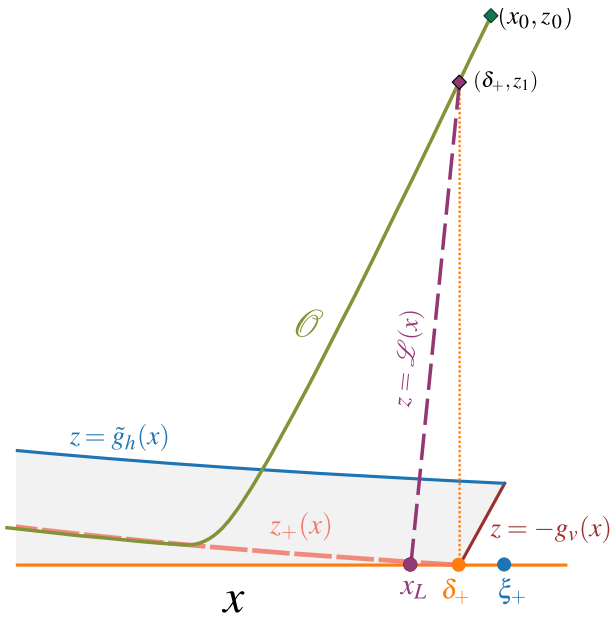

FIG. 11: Geometrical construction used in the proof of Case (C1) of Proposition 1.

We now prove that (30) holds for $x(t) \in [\delta_-, \delta_+]$. For this purpose, we distinguish two cases: (C1) $x_0 > \delta_+$ and (C2) $x_0 \leq \delta_+$.

Case (C1): Assume that $x_0 > \delta_+$.

Let (δ_+, z_1) denote the intersection point of the orbit $\mathscr{O}$ with $x = \delta_+$ (see Figure 11). Recall that δ_+ does not depend on μ. By the dependence of the solutions of ordinary differential equations with respect to parameters, one has

$$z_1 = z_1(\mu) = z_1(0) + O(\mu),$$

where

$$0 < z_1(0) < C - \delta_+ - g_v(\delta_+) = C - \delta_+ < \frac{C}{2}, \tag{31}$$

since $g_v(\delta_+) = 0$. Consider the line (magenta dashed line in Figure 11)

$$z = \mathscr{L}(x) := \frac{4C}{\delta_+}(x - \delta_+) + z_1,$$

which crosses $z = 0$ at

$$x = x_L := \delta_+ \left(1 - \frac{z_1}{4C}\right). \tag{32}$$

The slope of the vector field of system (20) at the points of $z = \mathscr{L}(x)$ for $x \in (x_L, \delta_+]$ is less or equal than the slope of the line itself. Indeed, for $\mu = 0$, we have

$$\frac{dz}{dx}\Big|_{z=\mathscr{L}(x),\mu=0} = \frac{4C}{\delta_+}\left(1 - \frac{\delta_+}{x}\right) + \frac{z_1}{x} - \frac{C}{L}(2\gamma - Lx)\frac{1}{x^2} < \frac{z_1 + C}{x} < \frac{z_1 + C}{\delta_+\left(1 - \frac{z_1}{4C}\right)} < \frac{\frac{C}{2} + C}{\delta_+\left(1 - \frac{1}{8}\right)} = \frac{12}{7}\frac{C}{\delta_+} < \frac{4C}{\delta_+}.$$

This implies that, for $x \in (x_L, \delta_+)$, the orbit $\mathscr{O}$ cannot cross the line $z = \mathscr{L}(x)$ and will intersect the curve $z = z_+(x)$ above this line. Moreover, for μ small, x_L satisfies $x_L > \frac{7}{4}\frac{\gamma}{L}$. Indeed, by (31), it follows that

$$x_L = \delta_+ \left(1 - \frac{z_1}{4C}\right) > \frac{\delta_+}{4}\left(3 + \frac{\delta_+}{C}\right) > \frac{7}{16}C > \frac{7}{4}\frac{\gamma}{L},$$

where it has also been used that $\frac{\delta_+}{4}\left(3+\frac{\delta_+}{C}\right)$ is an increasing function of δ_+ for $\delta_+ > 0$, that $\delta_+ > \frac{C}{2}$ and $\gamma < \frac{CL}{4}$. Notice that $\frac{7}{4}\frac{\gamma}{L} < x_b = \frac{2\gamma}{L}$, so x_L can potentially lie in both sides of x_b (see Figure 10 for a representation of x_b).

Let us consider $\eta > 0$ such that $x_b + 2\eta < \delta_+$. Then, we have the following two possibilities:

(a) Case $x_L > x_b + \eta$.

Recall that $z_+(x)$ also depends on μ. In order to put more emphasis on this dependence, we will write, when necessary, $z_+(x,\mu)$ instead of $z_+(x)$, and the same will be done for $\mathscr{L}$ and x_L.

Clearly, from its definition one has that

$$z_+(x,\mu) = \frac{2c(x)}{-b(x) + \sqrt{b^2(x) - 4a(x)c(x)}} = \frac{\gamma}{L^2}\frac{g_v(x)}{x - x_b}\mu + O(\mu^2), \tag{33}$$

for $x \in (x_b, \delta_+)$. Notice that since $x_L - x_b > \eta > 0$, we have

$$\frac{\gamma}{L^2}\frac{g_v(x)}{x - x_b} > 0, \qquad x_b + \eta < x < \delta_+. \tag{34}$$

Now, consider the equation

$$G(x,\mu) = \mathscr{L}(x,\mu) - z_+(x,\mu) = 0, \tag{35}$$

whose solution provides the intersection between the line $z = \mathscr{L}(x,\mu)$ and the curve $z = z_+(x,\mu)$. Solving this equation for $\mu = 0$ we have

$$G(x,0) = \mathscr{L}(x,0) - z_+(x,0) = \mathscr{L}(x,0) = 0 \qquad \Leftrightarrow \qquad x = x_L(0).$$

Moreover, $\frac{\partial G}{\partial x}(x_L, 0) = \frac{4C}{\delta_+}$.

Therefore, by the Implicit Function Theorem, there exists a solution $\tilde{x}(\mu)$ of $G(x,\mu) = 0$ of the form

$$\tilde{x}(\mu) = \tilde{x}(0) + O(\mu) = x_L + O(\mu).$$

Therefore, if $x(t) > \tilde{x}(\mu)$ one has that $\dot{z}(t) < 0$ (since the orbit $\mathscr{O}$ has not yet reached $z_+(x)$ and we know from Lemma 5(b) that, up to this point, $\dot{z} < 0$). Moreover, if $x(t) = \delta_-$ then $\dot{z}(t) > 0$ (see Lemma 5(a)). Since the interval $[\delta_-, \tilde{x}(\mu)]$ is compact, the function $z(t)$ has an absolute minimum

on it, and, by the previous properties, it has to be in the interior of the considered interval. This minimum must satisfy that $\dot{z}(t) = 0$ at it and, consequently, it must fall on the curve $z_+(x)$ (the curve $z_-(x)$ is negative in (δ_-, δ_+)).

Let us denote by $x_{\min}$ the x-component of the orbit $\mathscr{O}$ where this absolute minimum is reached.

Taking into account Lemma 4(b) we distinguish two possibilities:

(i) $x_{\min} \in (x_c, \tilde{x}(\mu)]$, with x_c introduced in Lemma 4(b). Then

$$z_+(x_{\min}) > M_{11} g_v(x_{\min})\mu.$$

Since $g_v(x)$ is a continuous function, there exists a constant $m_2 > 0$, independent of μ, such that $g_v(x) \geq m_1$ for any $x \in [x_c, \tilde{x}(\mu)]$. So, defining $M_3 := M_{11} m_2$ it turns out that

$$z(t) \geq z_+(x_{\min}) > M_3\mu,$$

when $x(t) \in [\delta_-, \delta_+]$, with M_3 independent of μ.

(ii) $x_{\min} \in [\delta_-, x_c]$. By the second part of Lemma 4(b), we have that

$$z(t) \geq z_+(x_{\min}) > M_6,$$

when $x(t) \in [\delta_-, x_c]$, with M_6 independent of μ. Obviously, if μ is small $M_3\mu < M_6$.

(b) Case $x_L \leq x_b + \eta$. First we check that, provided μ is small, the intersection of $z = \mathscr{L}(x)$ with $z_+(x)$ has x-component less or equal than $x_b + 2\eta$. Indeed, we prove it by *reductio ad absurdum*: if $x > x_b + 2\eta$ it follows that

$$\mathscr{L}(x) > \frac{4C}{\delta_+}(x_b + 2\eta - \delta_+) + z_1 = \frac{4C}{\delta_+}(x_L - \delta_+) + z_1 + \frac{4C}{\delta_+}(x_b + 2\eta - x_L) \geq \frac{4C}{\delta_+}\eta.$$

Moreover, by (33) and (34), $z_+(x) = O(\mu)$ in $[x_b + \eta, \delta_+)$ and then $z = \mathscr{L}(x)$ is above the curve $z = z_+(x)$, a contradiction.

Again, by Lemma 4(b), it turns out that $z_+(x) > M_3\mu$ in $[\delta_-, x_b + 2\eta]$, with M_3 independent of μ (using again that $M_3\mu < M_6$). The lower bound for $z(t)$ also follows when $x(t) \in [x_b + 2\eta, \delta_+]$ since $z(t)$ is a decreasing function on it.

Case (C2): Assume $x_0 \leq \delta_+$.

In this situation, there exists an orbit $\mathscr{O}' \in \mathscr{F}_\rho$ with initial condition $x(0) > \delta_+$ such that the $z(t)$-values of the orbit $\mathscr{O}$ are always above the $z(t)$-values of $\mathscr{O}'$. Applying case (C1) to $\mathscr{O}'$ leads to the bound for $\mathscr{O}$.

□

III. CONCLUSIONS

Bifurcations provide the mechanisms by which nonlinear systems undergo qualitatively changes in response to parameter variations. In recent decades, bifurcations have become a subject of growing interest in fields such as ecology [3, 5, 6, 10, 13], physics [21–24], and chemistry [25, 26]. A well-known phenomenon close to bifurcation consist of a slowing down of the dynamics, and so transients become extremely long [4–9, 11]. Moreover, the duration of transients typically follow universal scaling laws i.e., transient times typically scale with the parametric distance to the bifurcation value [2, 29]. Such scaling laws have been thoroughly analysed for local bifurcations [2, 29–32]. Interestingly, the well-known inverse square-root scaling law for the saddle-node bifurcation was identified experimentally in a Duffing oscillator implemented in an electronic circuit [22]. More recent research has investigated this scaling law in simple models with time delays i.e., delay differential equations [33], and under intrinsic noise [52]. The investigation of transient phenomena for global bifurcations in dissipative dynamical systems has received less attention, with the exception of the so-called chaotic crisis responsible for transient chaos [34–37].

Recent investigations of models in population dynamics have focused on the so-called quasi-neutral curves, which consist of a continuum of equilibria. In some cases, they or some subsets of them, are normally hyperbolic invariant manifolds (NHIMs) [42–44]. Usually, such manifolds exist only at the bifurcation value. When they are CQNE, depending on the initial condition, different asymptotic states are achieved. The dynamics tied to these CQNE has been investigated in mathematical models of allele fixation [45, 46], in models of sexual selection [48, 49], in two-species Lotka-Volterra competition systems [47], in epidemiology [50], and, more recently, in simple models of RNA transcription [51].

In this paper we have investigated transient phenomena arising upon a global bifurcation involving the emergence of a quasi-neutral manifold. To do so, we have considered a mathematical model describing the population dynamics of an auto-catalytic replicator with an obligate parasite. A similar scenario was found in a two-member hypercycle with an obligate parasite [53]. This dynamical system has three possible scenarios: (i) survival of the autocatalytic species and extinction of the parasite; (ii) co-existence of both species in a quasi-neutral scenario; and (iii) co-extinction. Scenario (ii) is structurally unstable since it exists only at the bifurcation value $K = L$ (K and L being the replication of the parasite and of the catalytic species, respectively). We have investigated transient dynamics at the vicinity of this global bifurcation, considering the cases $K \lesssim L$ and $K \gtrsim L$. We have identified what we call ghost CQNE: despite close to the bifurcation no CQNE is found, it still influences the orbits causing the delays. We have investigated the delays numerically, also providing analytical results on scaling phenomena above and below the bifurcation threshold.

Declaration of competing interests

The authors declare that they do not have any financial or nonfinancial conflict of interests.

CRediT authorship contribution statement

Ernest Fontich, Antoni Guillamon, J. Tomás Lázaro: Conceptualization, Formal analysis, Investigation, Supervision, Writing - original draft, Funding acquisition. **Tomás Alarcón**: Investigation, Supervision, Writing - original draft, Funding acquisition. **Blai Vidiella** : Methodology, Software, Investigation, Writing - original draft. **Josep Sardanyés**: Conceptualization, Methodology, Software, Investigation, Writing - original draft, Funding acquisition.

Acknowledgments

We also acknowledge support from MINECO and "Agencia Estatal de Investigación" grants RTI2018-098322-B-I00 (TA, JS), PGC2018-098676-B-100 (AG, JTL), RTI2018-098322-B-100 (AG) and AGAUR projects 2017SGR1049 (AG, JTL) and 2017SGR01735 (TA, JS). EF has been partially supported by the Spanish Government grant PID2019-104851GB-I00 (MICINN/FEDER,UE) and by the Catalan Government grant 2017-SGR-1374. BV, JS and TA have been partially funded by the CERCA Programme of the "Generalitat de Catalunya". BV has been also funded by grant RYC-2017-22243, whose PI is JS. JS has been also funded by a "Ramón y Cajal" contract (RYC-2017-22243). We also wish to acknowledge the hospitality of the research center "Laboratorio Subterráneo de Canfranc", where part of this research has been developed.

---

[1] Yuri A. Kuznetsov. *Elements of Applied Bifurcation Theory*. Number 112 in Applied Mathematical Sciences. Springer, Berlin, 2 edition, 1998.

[2] Steven H. Strogatz. *Nonlinear Dynamics and Chaos: With Applications to Physics, Biology, Chemistry and Engineering*. Westview Press, 2000.

[3] Max Rietkerk, Stefan C Dekker, Peter C De Ruiter, and Johan van de Koppel. Self-organized patchiness and catastrophic shifts in ecosystems. *Science*, 305(5692):1926–1929, 2004.

[4] Marten Scheffer. *Critical Transitions in Nature and Society*. Princeton University Press, 2009.

[5] A Carla Staver, Sally Archibald, and Simon A Levin. The global extent and determinants of savanna and forest as alternative biome states. *science*, 334(6053):230–232, 2011.

[6] Stephen R Carpenter, Jonathan J Cole, Michael L Pace, Ryan Batt, WA Brock, Timmothy Cline, Jim Coloso, James R Hodgson, Jim F Kitchell, David A Seekell, et al. Early warnings of regime shifts: a whole-ecosystem experiment. *Science*, 332(6033):1079–1082, 2011.

[7] Blai Vidiella, Josep Sardanyés, and Ricard Solé. Exploiting delayed transitions to sustain semiarid ecosystems after catastrophic shifts. *Journal of The Royal Society Interface*, 15(143):20180083, 2018.

[8] Alan Hastings, Karen C Abbott, Kim Cuddington, Tessa Francis, Gabriel Gellner, Ying-Cheng Lai, Andrew Morozov, Sergei Petrovskii, Katherine Scranton, and Mary Lou Zeeman. Transient phenomena in ecology. *Science*, 361(6406), 2018.

[9] Andrew Morozov, Karen Abbott, Kim Cuddington, Tessa Francis, Gabriel Gellner, Alan Hastings, Ying-Cheng Lai, Sergei Petrovskii, Katherine Scranton, and Mary Lou Zeeman. Long transients in ecology: theory and applications. *Physics of life reviews*, 32:1–40, 2020.

[10] Josep Sardanyés, Jordi Piñero, and Ricard Solé. Habitat loss-induced tipping points in metapopulations with facilitation. *Population Ecology*, 61(4):436–449, 2019.

[11] Blai Vidiella, Ernest Fontich, Sergi Valverde, and Josep Sardanyés. Habitat loss causes long transients in small trophic chains. *Theoretical Ecology*, pages 1874–1746, 2021.

[12] Robert M May, Simon A Levin, and George Sugihara. Ecology for bankers. *Nature*, 451(7181):893–894, 2008.

[13] Steven J Lade, Alessandro Tavoni, Simon A Levin, and Maja Schlüter. Regime shifts in a social-ecological system. *Theoretical Ecology*, 6(3):359–372, 2013.

[14] James D. Murray. *Mathematical Biology I. An Introduction*, volume 17 of *Interdisciplinary Applied Mathematics*. Springer, New York, 3 edition, 2002.

[15] Edward Ott. *Chaos in Dynamical Systems*. Cambridge University Press, 2002.

[16] Haye Hinrichsen. Non-equilibrium critical phenomena and phase transitions into absorbing states. *Advances in Physics*, 49(7):815–958, 2000.

[17] Géza Ódor. *Universality in nonequilibrium lattice systems: theoretical foundations*. World Scientific, 2008.

[18] M.K. Neilsen and H.L. Schreyer. Bifurcations in elastic-plastic materials. *International Journal of Solids and Structures*, 30(4):521–544, 1993.

[19] Sandra Kahan and Anibal C. Sicardi-Schifino. Homoclinic bifurcations in Chua's circuit. *Physica A: Statistical Mechanics and its Applications*, 262(1):144–152, 1999.

[20] Mikhail V. Ivanchenko, Eugene A. Kozinov, Valentin D. Volokitin, Alexey V. Liniov, Iosif B. Meyerov, and Sergey V. Denisov. Classical bifurcation diagrams by quantum means. *Annalen der Physik*, 529(8):1600402, 2017.

[21] L. Gil, G. Balzer, P. Coullet, M. Dubois, and P. Berge. Hopf bifurcation in a broken-parity pattern. *Phys. Rev. Lett.*, 66:3249–3252, Jun 1991.

[22] Stephen T Trickey and Lawrence N Virgin. Bottlenecking phenomenon near a saddle-node remnant in a Duffing oscillator. *Physics Letters A*, 248(2):185–190, 1998.

[23] Moumita Das, Ashkan Vaziri, Arshad Kudrolli, and L. Mahadevan. Curvature condensation and bifurcation in an elastic shell. *Phys. Rev. Lett.*, 98:014301, Jan 2007.

[24] Michael Gomez, Derek E. Moulton, and Dominic Vella. Critical slowing down in purely elastic “snap-through" instabilities. *Nature Physics*, 13(2):142–145, Oct 2016.

[25] Jerzy Maselko. Determination of bifurcation in chemical systems. An experimental method. *Chemical Physics*, 67(1):17–26, 1982.

[26] Peter Strizhak and Michael Menzinger. Slow passage through a supercritical Hopf bifurcation: Time-delayed response in the Belousov-Zhabotinsky reaction in a batch reactor. *The Journal of Chemical Physics*, 105(24):10905–10910, 1996.

[27] Lei Dai, Daan Vorselen, Kirill S. Korolev, and Jeff Gore. Generic indicators for loss of resilience before a tipping point leading to population collapse. *Science*, 336(6085):1175–1177, 2012.

[28] Hua-Guang Gu, Baobao Pan, Guanrong Chen, and Lixia Duan. Biological experimental demonstration of bifurcations from bursting to spiking predicted by theoretical models. *Nonlinear Dynamics*, 78:391–407, 10 2014.

[29] Edson D. Leonel. Defining universality classes for three different local bifurcations. *Communications in Nonlinear Science and Numerical Simulation*, 39:520–528, 2016.

[30] Rivania M.N. Teixeira, Danilo S. Rando, Felipe C. Geraldo, R.N. Costa Filho, Juliano A. de Oliveira, and Edson D. Leonel. Convergence towards asymptotic state in 1-D mappings: A scaling investigation. *Physics Letters A*, 379(18):1246–1250, 2015.

[31] Ernest Fontich and Josep Sardanyés. General scaling law in the saddle–node bifurcation: a complex phase space study. *Journal of Physics A: Mathematical and Theoretical*, 41(1):015102, dec 2007.

[32] Jorge Duarte, Cristina Januário, Nuno Martins, and Josep Sardanyés. Scaling law in saddle-node bifurcations for one-dimensional maps: A complex variable approach. *Nonlinear Dynamics*, 67:541–547, 01 2012.

[33] Joan Gimeno, Àngel Jorba, and Josep Sardanyés. On the effect of time lags on a saddle-node remnant in hyperbolic replicators. *Journal of Physics A: Mathematical and Theoretical*, 51(38):385601, aug 2018.

[34] C. Simó. On the Hénon-Pomeau attractor. *J. Stat. Phys.*, 21:465–494, 1979.

[35] Celso Grebogi, Edward Ott, and James A. Yorke. Chaotic attractors in crisis. *Phys. Rev. Lett.*, 48:1507–1510, May 1982.

[36] Mukeshwar Dhamala and Ying-Cheng Lai. Controlling transient chaos in deterministic flows with applications to electrical power systems and ecology. *Phys. Rev. E*, 59:1646–1655, Feb 1999.

[37] C. Grebogi, E. Ott, and J. Yorke. Fractal basin boundaries, long-lived chaotic transients, and unstable-unstable pair bifurcation. *Physical Review Letters*, 50:935–938, 1983.

[38] Celso Grebogi, Edward Ott, and James A. Yorke. Super persistent chaotic transients. *Ergodic Theory and Dynamical Systems*, 5(3):341–372, 1985.

[39] H. J. Wünsche, O. Brox, M. Radziunas, and F. Henneberger. Excitability of a semiconductor laser by a two-mode homoclinic bifurcation. *Phys. Rev. Lett.*, 88:023901, Dec 2001.

[40] Imre M. Jánosi, Leci Flepp, and Tamás Tél. Exploring transient chaos in an NMR-laser experiment. *Phys. Rev. Lett.*, 73:529–532, Jul 1994.

[41] T. L. Carroll, L. M. Pecora, and F. J. Rachford. Chaotic transients and multiple attractors in spin-wave experi-

ments. *Phys. Rev. Lett.*, 59:2891–2894, Dec 1987.

[42] N. Fenichel. Asymptotic stability with rate conditions. *Indiana Univ. Math. J.*, 23:1109–1137, 1974.

[43] N. Fenichel. Asymptotic stability with rate conditions II. *Indiana Univ. Math. J.*, 26(1):81–93, 1977.

[44] Stephen Wiggins. *Normally hyperbolic invariant manifolds in dynamical systems*. Applied mathematical sciences (Springer-Verlag New York Inc.); v. 105. Springer-Verlag, New York, 1994.

[45] Todd L. Parsons and Christopher Quince. Fixation in haploid populations exhibiting density dependence II: The quasi-neutral case. *Theoretical Population Biology*, 72(4):468–479, 2007.

[46] Todd L. Parsons, Christopher Quince, and Joshua B. Plotkin. Absorption and fixation times for neutral and quasi-neutral populations with density dependence. *Theoretical Population Biology*, 74(4):302–310, 2008.

[47] Yen Ting Lin, Hyejin Kim, and Charles Doering. Features of fast living: On the weak selection for longevity in degenerate birth-death processes. *Journal of Statistical Physics*, 148:646–662, 09 2012.

[48] I. Lorraine Heisler and James W. Curtsinger. Dynamics of sexual selection in diploid populations. *Evolution*, 44(5):1164–1176, 1990.

[49] P.B. Greenspoon and Sarah P. Otto. Evolution by fisherian sexual selection in diploids. *Evolution*, 63(4):1076–1083, 2009.

[50] Oleg Kogan, Michael Khasin, Baruch Meerson, David Schneider, and Christopher R Myers. Two-strain competition in quasineutral stochastic disease dynamics. *Phys. Rev. E*, 90:014301, 2014.

[51] Josep Sardanyés, Andreu Arderiu, Santiago Elena, and Tomás Alarcón. Noise-induced bistability in the quasineutral coexistence of viral RNA under different replication modes. *Journal Royal Society Interface*, 02 2018.

[52] Josep Sardanyés, Carles Raich, and T. Alarcón. Noise-induced stabilisation of saddle-node ghosts. *New Journal of Physics*, 22:093064, 2020.

[53] Josep Sardanyés and Ricard V. Solé. The role of cooperation and parasites in non-linear replicator delayed extinctions. *Chaos, Solitons & Fractals*, 31(5):1279–1296, 2007.